 doi:10.20944/preprints202111.0051.v1

Article

Correlated Bayesian Model of Aircraft Encounters in the Terminal Area Given a Straight Takeoff or Landing

Andrew Weinert[1,*], Ngaire Underhill[2], Christine Serres[3], and Randal Guendel[4]

[1] MIT Lincoln Laboratory; andrew.weinert@ll.mit.edu
[2] MIT Lincoln Laboratory; ngaire.underhill@ll.mit.edu
[3] MIT Lincoln Laboratory; christine.serres@ll.mit.edu
[4] MIT Lincoln Laboratory; randal.guendel@ll.mit.edu
* Correspondence: andrew.weinert@ll.mit.edu

Abstract: The incorporation of unmanned aircraft terminal operations into the scope of Detect and Avoid systems necessitates analysis of the safety performance of those systems—principally, an assessment of how well those systems prevent loss of well clear from and collision with other aircraft. This type of analysis has typically been conducted by Monte Carlo simulation with synthetic, statistically representative encounters between aircraft drawn from an appropriate encounter model. While existing encounter models include terminal airspace classes, none explicitly represents the structure expected while engaged in terminal operations, e.g., aircraft in a traffic pattern. The work described herein is an initial model of such operations, scoped at this time specifically for assessment of unmanned aircraft landings and encounters with other aircraft either landing or taking off. The model shares the Bayesian network foundation of other MIT Lincoln Laboratory encounter models but tailors those networks to address structured terminal operations, i.e., correlations between trajectories and the airfield and each other. This initial model release is intended to elicit feedback from the standards-writing community.

Keywords: aviation; modeling; simulation; safety; standards; terminal; unmanned

DISTRIBUTION STATEMENT A. Approved for public release. Distribution is unlimited.. This material is based upon work supported by the Federal Aviation Administration under Air Force Contract No. FA8702-15-D-0001. Any opinions, findings, conclusions or recommendations expressed in this material are those of the author(s) and do not necessarily reflect the views of the Federal Aviation Administration. Delivered to the U.S. Government with Unlimited Rights, as defined in DFARS Part 252.227-7013 or 7014 (Feb 2014). Notwithstanding any copyright notice, U.S. Government rights in this work are defined by DFARS 252.227-7013 or DFARS 252.227-7014 as detailed above. Use of this work other than as specifically authorized by the U.S. Government may violate any copyrights that exist in this work.

1. Introduction

The continuing integration of uncrewed aircraft system (UAS) operations into the National Airspace System (NAS) requires new or updated regulations, policies, and technologies to maintain safety and enable efficient use of the airspace. One such technology is detect and avoid (DAA), which enables uncrewed aircraft to comply with applicable operating rules of Title 14 of the Code of Federal Regulations (14 CFR). These rules include Part 91, §.3, .111, .113(b), .115, .123, and .181(b), which prescribe that aircraft must remain well clear from and prevent a midair collision (MAC) with other aircraft.

DAA is part of a multi-layered airspace conflict management architecture and DAA is often not employed until prior strategic mitigations have failed[1]. While there is a singular standard for crewed aircraft collision avoidance, there are a variety of standards for UAS DAA systems. DAA standards are primarily organized by size of the aircraft;

 doi:10.20944/preprints202111.0051.v1

expected operations by airspace class or altitude; and how prescriptive the standard is written.

A foundational element to these standards is modeling and simulation activities to design and evaluate the safety and suitability of a DAA system. Monte Carlo simulations in particular enable surveillance systems and algorithms to be tested under an exhaustive set of circumstances not possible through live flight testing. The simulations are often validated through human-in-the-loop experiments and flight testing. For example, an update to the standard prescribing a collision avoidance system for crewed aircraft was validated in part using this approach[2].

1.1. Motivation

RTCA Special Committee (SC)-228 is developing performance standards for a variety of UAS technologies, with DAA standards being developed in multiple phases[3]. Phase one focused on enabling UAS transit operations in Class D and G airspaces when flying to/from Class A airspace or special use airspace. This phase was based on guidance from the U.S. UAS Executive Committee Science and Research Panel[4]; validated primarily in simulation[5]; and published as the DAA Minimum Operating Performance Standards (MOPS), DO-365 revision A[6]. Phase two included UAS expanded en route operations with new types of sensors, along with take-off and landing operations in some terminal airspaces. Phase two has been published as DO-365 revision B in 2021, and example implementations include the DAIDALUS[7] and ACAS Xu DAA systems[8]. Phase three activities will initiate in 2021 and address more specialized UAS operations that require more tailored performance or constrained guidance, such as operations in Class B airspace or vertical takeoff and landing operations for advance air mobility (AAM) use cases.

Across all RTCA SC-228 phases, the MIT Lincoln Laboratory (MIT LL) statistical encounter models have been used to model aircraft behavior. These are trained on real-world observations of individual aircraft or observations of encounters between two aircraft. The majority of these models are uncorrelated[9]–[12], which assume that the aircraft are not participating in the air traffic control system and their behavior is independent of other aircraft. For encounters in the terminal environment, such as considered by RTCA SC-228, a correlated encounter model was required that assumes that aircraft behavior and the relatively geometry between aircraft was dependent upon an air traffic service. While MIT LL previously developed[13] and updated[14] a correlated model, it was designed to model encounters that occur away from airports in terminal airspaces, or while one or both aircraft are merely passing through the terminal airspace. This previous model did not represent the standardized approach and departure routes that describe the permissible flight paths for large airports, or smaller airports employing a standardized flight pattern to regulates flow into and out of the airport. In response, a new correlated model that better represents the structure and encounter dynamics of the terminal airspace was required to support RTCA SC-228 and the evaluation of DAA systems.

1.2. Scope

The model development scope was directly informed by the terms of reference of RTCA SC-228[3], specifically those associated with phase two activities for DAA MOPS development. This standard was designed for UAS weighing greater than 55 pounds and whose maximum dimensions are likely greater than 25 feet. Considered was geographically limited operations and operations within a terminal environment, which include: Class D airspace, towered airfields within Class E airspace, nontowered airfields within Class E airspace, non-towered airfields within Class G airspace, take-off and landing operations in Class C, D, E, and G airspace, and off-airfield launch and recovery sites within Class G airspace. To support RTCA SC-228, we assume UAS land via a straight-in instrument approach or an analogous departure route.

Preprints (www.preprints.org) | NOT PEER-REVIEWED | Posted: 2 November 2021 doi:10.20944/preprints202111.0051.v1

RTCA SC-228 defined the terminal environment as within 8 nautical miles laterally and 3000 feet vertically of a runway. We adopted a slightly larger definition of 8 nautical miles laterally and 5000 vertically of a runway. Within this environment, we defined an encounter as when two aircraft are within 4 nautical miles laterally and 2000 feet vertically of each other for at least one second. Aircraft must overlap in time for at least thirty seconds too. Notably this volume is larger than the volume for many Class C and D airspaces; thus, the defined terminal environment may consist of multiple airspace classes for a specific airport. For example, the terminal environment for a notional airport in Class D airspace will consist of the Class D airspace within 2.5 nautical miles and up to 2500 feet AGL from the airport; along with the surrounding Class G airspace.

Out of scope use cases included very low level UAS operations exclusively below 500 feet AGL; high altitude Class E above A operations; and 14 CFR Part 135 cargo operations. Some of these out of scope concepts are being addressed through RTCA SC-147[15] and ASTM F38[16]. These out of scope efforts leverage different MIT LL encounter models.

1.3. Objectives and Contributions

The primary objectives were to develop a statistical model that represents aircraft behavior in the terminal environment and then sample this model to create an encounter set to support RTCA SC-228 safety analyses. Since terminal airspaces can be traffic dense, the developed model needed to be cognizant of the airspace structure that provides implicit coordination and communicates intent amongst all the airspace users. Although every airport is different and traffic patterns likewise vary, assessing encounters specific to the traffic at one airport would not be sufficient to deem a DAA system safe for terminal operations at all airports. Traffic patterns may be tailored to account for various configurations of runways as well as external factors like surrounding terrain or other natural or man-made features

Accordingly, the primary contribution was a set of Dynamic Bayesian models representative of single runway airports in Class C, D, or E/G airspace and potentially representative of Class B. These models characterized the interaction between two aircraft. One aircraft must be either on a straight-in approach or straight-out departure while the other can approach or depart without restrictions, along with simply transiting through the airspace. Similar to other recently developed models[17], this terminal model considered the type of aircraft (e.g. fixed-wing, rotorcraft, etc.). Additionally, while trained solely on observations of crewed aircraft, the model can be sampled such that the dynamics and behavior of one modeled aircraft is a surrogate for a large UAS. These models were released as open source software in July 2021[18], with software to sample the models released in October 2021[19].

The primary contribution was preceded by an initial prototype model (version 1.0) narrowly scoped to aircraft on straight-in approach to a Class D single runway airport encountering a second aircraft either landing or taking off; and a subsequent prototype (version 2.0) that added Class E/G single runway airports, straight-out departures, and transiting aircraft. A dataset of sampled encounters using the version 1.0 was publicly released, but the Bayesian models for the two prototypes were not made publicly available. Only version 3.0 was released as open source software[18], [19]. None of the models, as of October 2021, fully represent all airport or terminal environment use cases; and development is ongoing.

A secondary contribution was an analysis of which data source to leverage for model training, with specific consideration for spatial extent and transponder equipage. Some of the software and data developed for this effort have been released under permissive open source licenses.

2. Materials and Methods

Preprints (www.preprints.org) | NOT PEER-REVIEWED | Posted: 2 November 2021 doi:10.20944/preprints202111.0051.v1

This section overviews the training datasets; how aircraft intent was classified in the terminal environment; how the models were trained; and rejection sampling approach used when sampling the models to create encounters. Encounters consist of two aircraft, with the first aircraft referred to as the ownship and the other aircraft referred to as the intruder. For DAA evaluations, we assume ownship to be a UAS. Specifically, for evaluations related to RTCA SC-228 DO-365B, we assumed the UAS to be operating under Instrument Flight Rules (IFR); however, we enforce this when sampling, not when training, the model. Many, not all, of our assumptions were derived from DO-365B. Important assumptions for developing and training the model included:

- An encounter is when ownship and intruder are within 4 nautical miles laterally and 2000 feet vertically of each other for at least one second over at least a thirty second duration;
- Ownship is on a straight-in takeoff or approach;
- Intruder aircraft may be landing, taking off, or transiting the area;
- Intruder aircraft may not be landing or taking off from a nearby airport;
- Sampled trajectories are constrained to within 8 NM of the airfield and 5000 ft above airfield elevation (minimum altitude is 200 ft above airport elevation); and
- Sampled trajectories are a maximum of 300 seconds long.

The trained models align with the Bayesian network framework of other MIT LL encounter models[10] but are reformulated to account for the structured behavior aircraft employ when landing or taking off. Like the existing radar-based en route correlated encounter model[14], this terminal encounter model represents the relative geometry of two aircraft. While the other correlated model defined relative geometry based on the horizontal and vertical separation between aircraft, the geometry of this terminal encounter model was based on the relative geometry between each aircraft and the runway.

Notably, our approach also does not identify and model turning points, a concept popularized by Gariel et al.[20]. Mahboubi and Kochenderfer[21] demonstrated that a turning point model performs well on simulated data; due to its reliance on noisy heading rates, it has difficulty with real-world data. Our approach also differs from Barrett[22] et al. who used an unsupervised cluster algorithm to identify departure and approach procedures and fit the clusters to a generative model based on intra-cluster covariance matrices. Barrett[22] et al. was inspired by the clustering approach previous proposed by Li et al.[23], [24]. Similar to these other efforts, we also do not leverage filed or amended flight plans like Krozel[25] or Georgiou et al.[26]. Additionally, we did not consider aircraft trajectories on the surface, such as Churchill and Bloem[27].

Instead, our approach clustered and classified tracks based on assumptions of airport design, approach and departure routes, and aviation heuristics, such as the 1 in 60 rule (one degree offset angle equates to one nautical mile displacement at 60 nautical miles from a origin). Additionally, we did not employ unsupervised learning techniques as we wanted to take advantage of known physical states during takeoff or landing operations. Namely, aircraft taking-off or landing should have a low AGL altitude when close to the runway and that aircraft transiting over the airport would do so at higher altitudes. Consequently, our approach was computationally efficient, enabling us to train a model based on billions of observations. Furthermore, RTCA SC-228 and the immediate users of the developed model, expressed a preference for the newly trained model to be consistent with previous encounter models for improved usability, which resulted in using a similar Bayesian framework. Specifically, our approach consists of the following:

1. Download and pre-process (i.e. interpolate, outlier detection etc.) training data
2. Coarsely spatially filter training data to terminal airspace
3. Classify track intent (e.g. landing, taking-off, transiting) for training data within terminal airspace
4. Given classified tracks, identify encounters between aircraft
5. Train model using identified encounters
6. Sample model to create representative encounters

2.1. Training Data

Two sets of data were used to train two separate encounter models: 1) FAA collected terminal radar track data over the period January through September 2015 at select airports throughout the NAS and 2) 190+ days of data over the period January 2019 through February 2020 from the OpenSky Network, a database consisting of ADS-B and Mode S reports[28]. These two sources of data have different assumptions and surveilled different types of aircraft. Training multiple models enabled us to assess the sensitivity of the models to different biases, while mitigating some weakness for a given dataset. Biases include the type of aircraft observed, the metadata associated with each surveilled track, or surveillance error. Data near fixed-runway airports in Class C, D, E, and G airspaces were in scope for version 3.0 of the model, while Appendix A lists the airports that were in scope for version 2.0 of the model. As noted in Section 1.3, the focus of this paper is version 3.0.

The terminal area radars data provided to MIT LL included standard aviation transponders with Mode A, C, and S capabilities. The OpenSky Network surveils aircraft only equipped with ADS-B, where ADS-B aircraft also generally support Mode C while not all Mode C aircraft are also equipped with ADS-B. However, the terminal area radars have a more limited spatial and temporal scope, whereas the OpenSky Network has better theoretical surveillance coverage. Additionally, the OpenSky Network was freely and easily available whereas the terminal area radar data was not.

2.1.1. OpenSky Network

Observations of crewed aircraft were sourced from the OpenSky Network[28], a community network of ground-based sensors that observe aircraft equipped with Automatic Dependent Surveillance-Broadcast (ADS-B) Out. The OpenSky Network offers a historical database using Cloudera Impala. It is a full database requiring terabytes of storage. Impala is a distributed query engine and does not index structures for query optimization. Queries can be formulated based on mean sea level (MSL) altitude, time, latitude, longitude, and the ICAO 24-bit address. The raw observations are only in MSL altitude and the OpenSky Network does not estimate the AGL altitude for any observations. Observations can be one second apart. In response, we developed and publicly released the software, em-download-opensky[29], to generate queries based on above ground level altitude, location of airports, airspace class, and time zones. Using this software, we generated 136,884 queries for 196 days across 695 bounding boxes across Class B, C, and D airspace across the United States. Temporally, we queried for the first 14 days of each month from January 2019 through February 2020. This time window was largely unaffected by the COVID-19 pandemic, as the Schengen Area travel ban didn't take effect until March 2020[30].

Prior to model training, the OpenSky Network data was (1) parsed and organized; (2) archived; and (3) processed and interpolated into track segments[31]. Processing included removing track segments with less than ten observations; calculating the above ground level altitude was calculated; identifying airspace class; and estimating dynamic rates (e.g. vertical rate) were calculated. Once processed, track segments were ready for model training. For details on how this dataset was curated and processed, please see [32] where this dataset is referred to as the aerodrome dataset.

The aerodromes dataset differed from the Mondays dataset, that was curated from the OpenSky Network to train the recent uncorrelated encounter models [32]. The Mondays dataset was curated from OpenSky Networks from 104 Mondays spanning from 2018-02-05 to 2020-11-16; not all Mondays in this span were included. The software used to query the OpenSky Network for the aerodromes dataset has been released as open source software [29]. This dataset was not spatially limited to regions around airports but had a more restrictive temporal scope of just Mondays. The COVID-19 pandemic was also in scope for this dataset. The Mondays dataset was continued expanded upon after model development, as of August 2021 the Mondays dataset now consists of Mondays through 2021-08-02.

Preprints (www.preprints.org) | NOT PEER-REVIEWED | Posted: 2 November 2021 doi:10.20944/preprints202111.0051.v1

2.1.2. Terminal Area Radars

Observations of crewed aircraft were sourced from raw secondary radar reports from terminal radars (ASR-9) that participated in the TCAS RA Monitoring System (TRAMS) from January through September 2015. Radars included the ASR-9 located at MIT LL and radars associated with the following airports: KATL, KDEN, KDFW, KFLL, KHPN, KJFK, KLAS, KLAX, KOAK, KORD, KPDX, KPHL, KSDF, KSEA, KSTL. The specific radar identifiers were respectively: ATL, DEN, DFW, FLL, HPN, JFK, LAS, LAX, LAXN, MOD, OAK, ORDA, PDX, PHL, PHX, SDF, SEA, STL. These radars support the TCAS Operational Performance Assessment (TOPA) program that was established over a decade ago[33]. While TOPA is ongoing program, the data made available to support model development varied in quantity and temporal scope. For example, KDFW had data from January through August while KOAK only from June through August.

These radar reports provide latitude, longitude and barometric altitude for transponder-equipped aircraft within the radar's surveillance volume. All of these radars were located within a Mode C veil, where aircraft, with few exemptions, are required to be transponder-equipped. While these radars surveil standard aviation transponders, not all surveillance information was made available to MIT LL. Specifically, the Mode S address was not included in this dataset, preventing classification of aircraft type using aircraft registries. This proximity to a large airport was a source of biases for this training data, which we further discuss in Section 2.2.

2.1.3. Altitude and Airspace Class Characterization

To identify potential biases in the training data, we characterized the different datasets, leveraging software and a methodology previously described in [34]. This characterization was also important in assessing if the different training datasets were similar or different and if there was a sufficient difference between datasets to warrant training a model with each dataset. For each dataset, the altitude distributions given airspace class was calculated using all latitude, longitude, and barometric altitude reports using the workflow described in [31]. Unlike [34], we did not consider the number of seats onboard the aircraft, as we lacked the metadata in the terminal area radar dataset required for that characterization. Figure 1 illustrates the distribution for the OpenSky Network aerodromes dataset, Figure 2 for the terminal area radar dataset, and for comparison, Figure 3 is the distribution of the "Mondays" dataset used for the recent uncorrelated encounter models. Note that the limit of the y-axis is greater in Figure 1 than Figures 2-3, due to the terminal area radar dataset being significantly larger. Table 1 reports that each dataset had billions of interpolated observations of aircraft at altitudes below 5,000 feet AGL, based on barometric altitude reports, and prior to any spatial filtering performed as part of model training. To calculate Table 1 and Figures 1-3, the computations were paralleled across 1007 xeon-e5 processes on the LLSC TX-Green. Computations required an hour or less for all datasets, if computed serially without parallelization, an estimated 16.1 (aerodromes), 31.7 (Mondays), 980.7 (terminal area radars) hours would had been required.

Table 1. Data points below 5,000 feet AGL for each dataset, organized by airspace class.

Airspace	Mondays	Aerodromes	Terminal Area Radars
Class B	251,671,725	505,322,452	1,026,076,842
Class C	79,874,269	108,969,262	126,863,443
Class D	57,887,219	81,304,346	214,349,345
Other	667,255,320	696,368,992	2,282,086,215
Total	*1,056,688,533*	*1,391,965,052*	*3,649,375,845*

First, note that in Figures 1-3 the Class C and D distributions taper off at 2500 and 4000 feet AGL, the nominal ceilings for the respective airspace classes. Regardless of airspace class, the majority of observations were above 500 feet AGL. The peak in all figures between 500 and 1000 feet was hypothesized to aircraft trying to maintain an al-

Preprints (www.preprints.org) | NOT PEER-REVIEWED | Posted: 2 November 2021 doi:10.20944/preprints202111.0051.v1

titude below the nominal Class E floor of 700 feet AGL or the Class G ceiling of 1,200 feet AGL. The decrease in observations at 3000 feet AGL and upward can be partly attributed to behavior induced by 14 CFR § 91.159 that regulates the hemispheric flight rules and when VFR must navigate using MSL altitude. This was especially evident in the terminal area radars dataset. We also hypothesized the peak between 1500-2000 feet AGL could be attributed to general aviation cross-country operations, but no analysis was conducted to make a definitive conclusion.

Next, by comparing the figures, we observed that the terminal area radar dataset (Figure 1) had the most observations, below 1000 feet, in Class B and other airspaces, followed by the aerodromes dataset (Figure 2) and lastly by the "Mondays" dataset (Figure 3). As the terminal area radars were largely co-located at Class B airports, this was expected. The aerodromes dataset had the most observations for the Class C and D airspaces. At higher altitudes, there was less of a difference between the terminal area radar and aerodrome datasets for Class B but the terminal area radars consistently had significantly more observations for the other airspace classes.

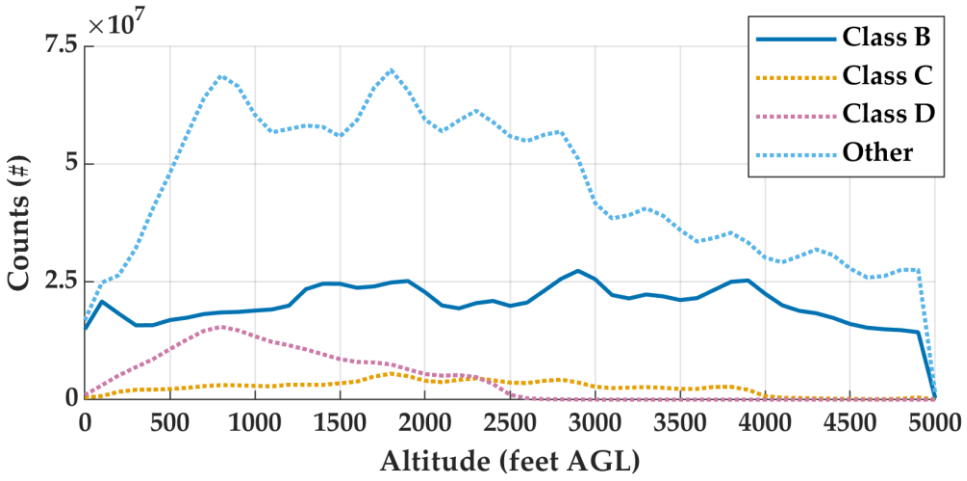

Figure 1. Altitude and airspace distributions below 5,000 feet AGL for the terminal area radars dataset.

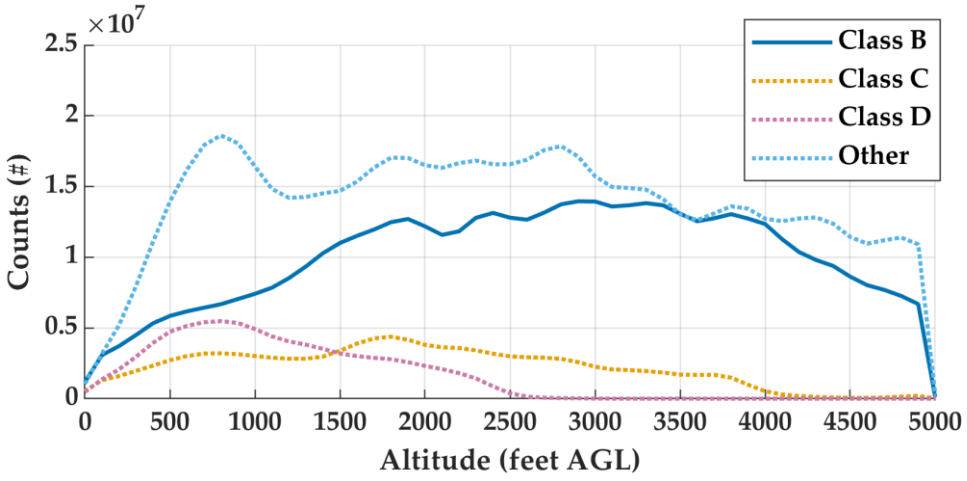

Figure 2. Altitude and airspace distributions below 5,000 feet AGL for the OpenSky Network aerodromes dataset.

Preprints (www.preprints.org) | NOT PEER-REVIEWED | Posted: 2 November 2021 doi:10.20944/preprints202111.0051.v1

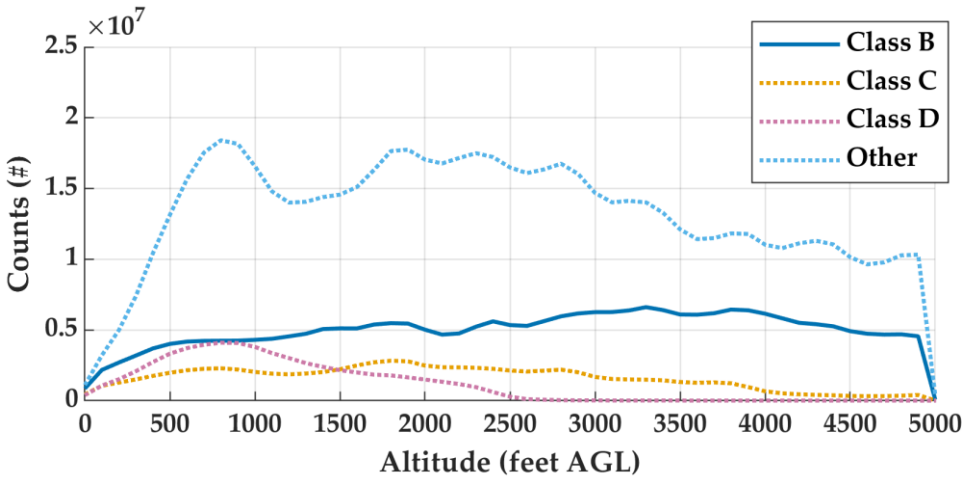

Figure 3. Altitude and airspace distributions below 5,000 feet AGL for the Mondays dataset used to train the OpenSky Network-based uncorrelated encounter models.

Since the model encompassed the airspace within 8 nautical miles of the airport, identified encounters can cross multiple airspaces, as noted in Section 1.2. Generally below 1200 feet AGL, Class C and D airspaces extend 2.5-5 nautical miles from a controlled runway. Given our encounter range criteria of 4 nautical miles, an encounter could occur when one aircraft was in Class D airspace and another in other airspace. An aircraft could also transition between airspaces over the course of the 30 second encounter duration. Thus, the significantly more observations of aircraft in other airspace at low altitudes was advantageous for the terminal radar dataset. The terminal area radar dataset had the most observations for a given location, if lower altitude surveillance was available, but this dataset was also the most restricted spatially and temporally.

Furthermore, when comparing the two OpenSky Network-based datasets, the percent difference between datasets for Class E and G (other) airspace was only 4.27%, yet it was 30% or greater for the other airspace classes. These percent differences demonstrate the advantage of curating a dataset, based on areas of interest, by querying the OpenSky Network. While the "Mondays" dataset has theoretically the best spatial coverage, as all data observed in the United States is in scope for that dataset, the OpenSky Network does not have universal low altitude coverage across the United States. The OpenSky Network has significant coverage gaps in rural or low population areas. However, these regions also typically have a low density of crewed aircraft traffic and these coverages gaps are not a significant impediment for model training. Accordingly, the wider temporal scope of the aerodromes dataset and surveillance of more types of transponders with the terminal area radar dataset results in these datasets having more observations than the "Mondays" dataset. The "Mondays" dataset also included 2018, when fewer aircraft were equipped with ADS-B and fewer sensors were participating in the OpenSky Network, and 2020 when aviation activity sharply decreased due to the COVID-19 pandemic[30].

2.2. Initial Spatial Filtering

All track segments at least 30 seconds in duration (assuming one second updates), within a 10 NM radius of an airport of interest, and up to 4,000 ft altitude relative to the airport surface were identified as within the vicinity of an airport. The FAA airport open dataset[1] was used to define the latitude and longitude coordinates of the airports. Additionally, observations with transponders squawking specific special use transponder

[1] https://ais-faa.opendata.arcgis.com/datasets/e747ab91a11045e8b3f8a3efd093d3b5_0

Preprints (www.preprints.org) | NOT PEER-REVIEWED | Posted: 2 November 2021 doi:10.20944/preprints202111.0051.v1

codes, such as those reserved for law enforcement aircraft, were also filtered out. Refer to Appendix B for a complete list of these codes. Tracks that did meet all these conditions were filtered out and not considered in the subsequent processing. Parallelized across 1008 xeon-e5 processes on the LLSC TX-Green with a block task distribution, 782 seconds was required to identify 19,293,916 OpenSky ADS-B tracks and 10,045 seconds for 36,701,193 terminal radar Mode C tracks.

The initial spatial filtering was primarily executed to reduce the computational complexity and requirements for other processing steps. The quantity of data reported in Table 1 is not a good indicator of where encounters were identified for model training.

2.2.1. Data per National Plan of Integrated Airport Systems

Table 2 reports the data identified as spatial filtering for select airports. For each airport, we also noted if the airport was designated as a primary airport in the 2015-2019 FAA National Plan of Integrated Airports Systems (NPIAS)[35]. Primary airports are grouped into categories of large (L), medium (M), small (S), and nonhub (N). Large hubs are those airports that each account for at least 1% total U.S. passenger enplanements; while nonhub primaries enplane less than 0.05% of all commercial passenger enplanements but have more than 10,000 annual enplanements. Medium and small hubs are grouped between large and nonhub primaries.

Table 2. Total track points after initial spatial filtering for select airports.

FAA ID	Class	Hub	OpenSky Network	Terminal Area Radar
BOS	B	L	10,881,938	13,270,494
ABE	C	N	1,816,670	2,285,593
BUR	C	M	16,789,410	29,748,003
FLL	C	L	10,342,130	50,856,891
SMF	C	M	6,876,029	0
XNA	C	S	1,466,794	0
ACK	D	N	21,934	0
ADS	D	-	20,954,315	68,151,579
BED	D	N	2,740,664	6,220,588
EYW	D	S	0	0
MVY	D	N	820,654	0
RNT	D	-	21,892,547	46,653,226
TTD	D	-	5,360,106	14,106,809
7N7	E/G	-	7,968,295	18,523,179
17N	E/G	-	2,252,995	13,006,900
19N	E/G	-	5,818,462	18,784,328
DDH	E/G	-	0	0

As hubs increased in enplanements, we generally identified more potential tracks; although there was not a strong correlation. The quantity of data was dependent more on the surveillance source, which likely has some correlation with NPIAS categorization. For example, Addision Airport (ADS), a nonprimary national airport, had one of the largest datasets. The size of the ADS dataset however was due to ADS located in the vicinity of Dallas Love Field (DAL) and Dallas Fort Worth International (DFW) which are medium and large hubs, respectively. Additionally, more data was available for BED and ABE, nonhub primaries, than XNA or EYW, small hubs. These four airports all had less data identified than Oldsman Township Airport (7N7), a non-towered single runway airport approximately 10 nautical miles from Philadelphia International. However, the majority of the tracks identified near 7N7 failed to satisfy the runway or encounter criteria described in subsequent sections.

2.2.2. Joint Distributions of Relative Distance and Altitude

Preprints (www.preprints.org) | NOT PEER-REVIEWED | Posted: 2 November 2021 doi:10.20944/preprints202111.0051.v1

In addition to Tables 1 and 2, we calculated the joint distributions of the relative distance and altitude between the airport and all the nearby data. The joint distributions are visualized as contours. While the initial filtering includes altitudes up to 4000 feet relative to the airport, the contours are illustrated with relative altitude up to 2500 feet for readability and to promote discussion about the lower altitudes, which are of greater interest. By reviewing the joint distributions for specific airports, we can assess the potential local geospatial biases of the different datasets and visualize the surveillance coverage of each dataset.

For example, Figure 4 illustrates the relative distance distributions for Renton Municipal (RNT), a single runway Class D airport about 4 nautical miles northeast of Seattle-Tacoma International (SEA). These support colloquial statements such as "5% of the identified traffic based on the OpenSky Network near RNT was within 2 nautical miles and 1000 feet or less of the airport," or "50% of the identified traffic based on the terminal area radar dataset was at least 6 nautical miles and 500 feet above RNT."

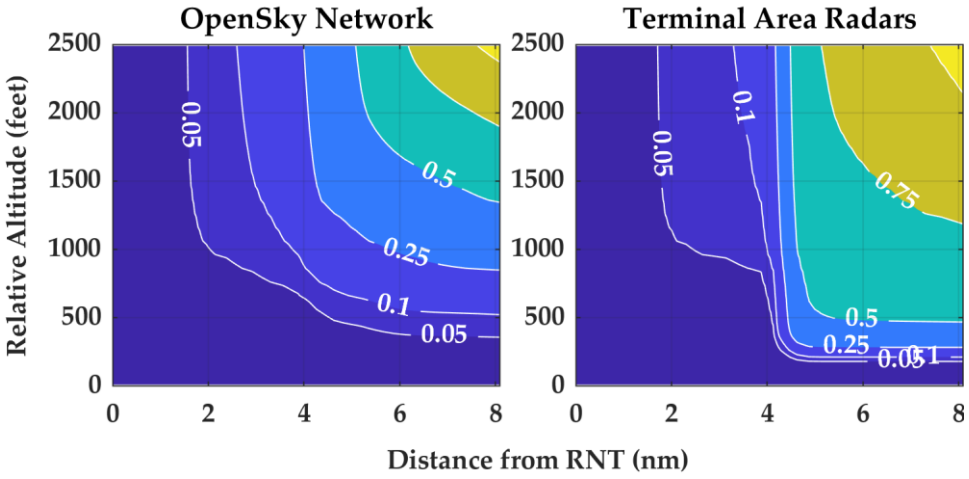

Figure 4. Fraction of aircraft positions relative to RNT.

RNT exemplifies the effect of nearby airports on identified tracks. Because the OpenSky Network is a distributed network of sensors, there was potentially less of an observation bias towards one specific location. This bias was exemplified by the gradual gradient around 4 nautical miles from the OpenSky Network-based tracks and the steep gradient from the terminal area radars dataset. The terminal radar located at SEA was expectantly observing very low altitude traffic operating to and from SEA. Section 2.3 will discuss how the nearby airport traffic will be filtered out prior to model training.

However not all low altitude traffic can be attributed to nearby airports. Of the more than 21 million points from the OpenSky Network dataset near RNT, 921,958 or about 4%, were associated with rotorcraft. Similarly, about 4% and 6% of OpenSky Network-based data were rotorcraft for FLL and ADS, yet 12% and 15% were rotorcraft for BED and SMF. The tendency for rotorcraft to operate at lower altitudes has also been observed with the uncorrelated encounter models [12].

Preprints (www.preprints.org) | NOT PEER-REVIEWED | Posted: 2 November 2021 doi:10.20944/preprints202111.0051.v1

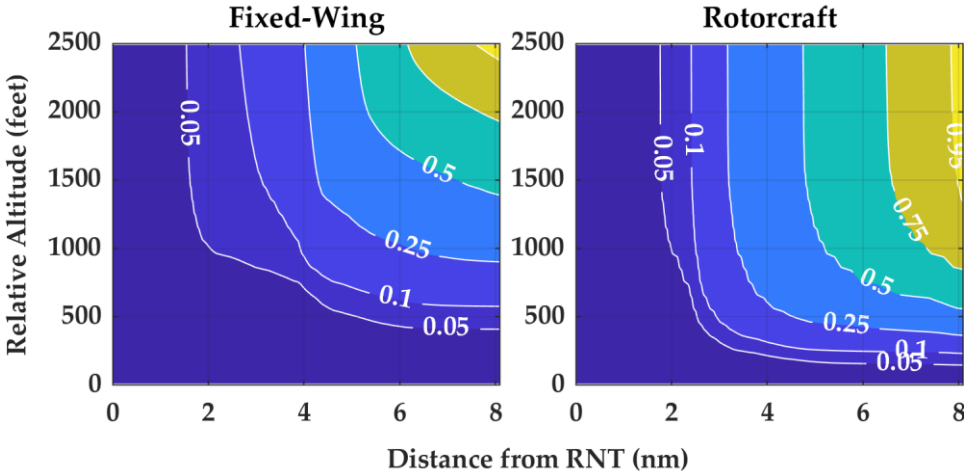

Figure 5. Fraction of aircraft positions based on the OpenSky Network relative to RNT, organized by aircraft type.

Relative location to the terminal radars was a source of bias, and sensor location was also a bias with the OpenSky Network. ACK and MVY are the Class D airports respectively for Nantucket and Martha's Vineyards, islands off the southern coast of Massachusetts. They are more than 50 nautical miles from the nearest terminal area radar and about 26 nautical miles apart from each other. Due to the distance away from the terminal radars, it was expected that neither airport would have any processed tracks from that dataset. As offshore islands, they are a good example of some the advantages and disadvantages of crowdsourced data. Foremost, particularly with MVY, the OpenSky Network provided hundreds of flight hours for ADS-B equipped aircraft for a location where the other dataset had no coverage. However, these crowdsourced sensors often have limited range, which is exemplified by comparing the distance contours for ACK and MVY. These contours suggested that a sensor was located on Martha's Vineyard, as MVY had relatively good low altitude coverage but that all observations over Nantucket were also from this MVY-based sensor. There was substantially less data near ACK and a bias towards higher altitudes.

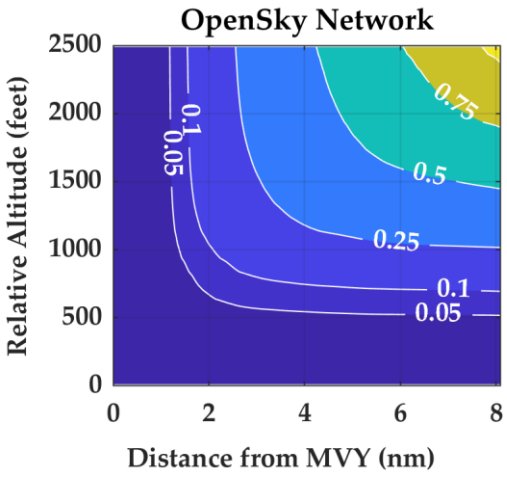

Figure 6. Fraction of aircraft positions relative to MVY. No data was available in the terminal area radars dataset.

Preprints (www.preprints.org) | NOT PEER-REVIEWED | Posted: 2 November 2021 doi:10.20944/preprints202111.0051.v1

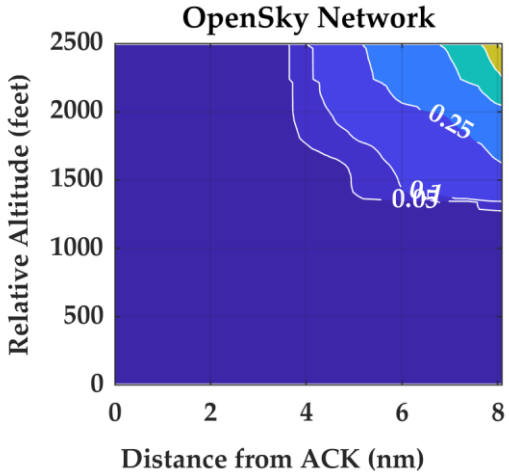

Figure 7. Fraction of aircraft positions relative to ACK.

Similar to MVY and ACK, the importance of sensor location is also illustrated by the distributions for Lehigh Valley International (ABE), a Class C airport in Pennsylvania about 40 nautical miles north of Philadelphia, PA and 60 nautical miles west of Newark, NJ. Table 2 reports that the terminal radar dataset had at least 450,000 observations, within 10 nautical miles and 4000 feet of ABE, more than the OpenSky Network-based tracks. However, the following figure illustrates that nearly all the terminal radar-based tracks are at least 1,5000 feet above ABE, while the OpenSky Network had significantly better low altitude coverage of the region. This would ultimately result in no encounters identified for model training with the terminal radar dataset while encounters were identified using the OpenSky Network-based dataset. Similar trends were exhibited with Hollywood Burbank (BUR), a Class C airport serving northern greater Las Angeles.

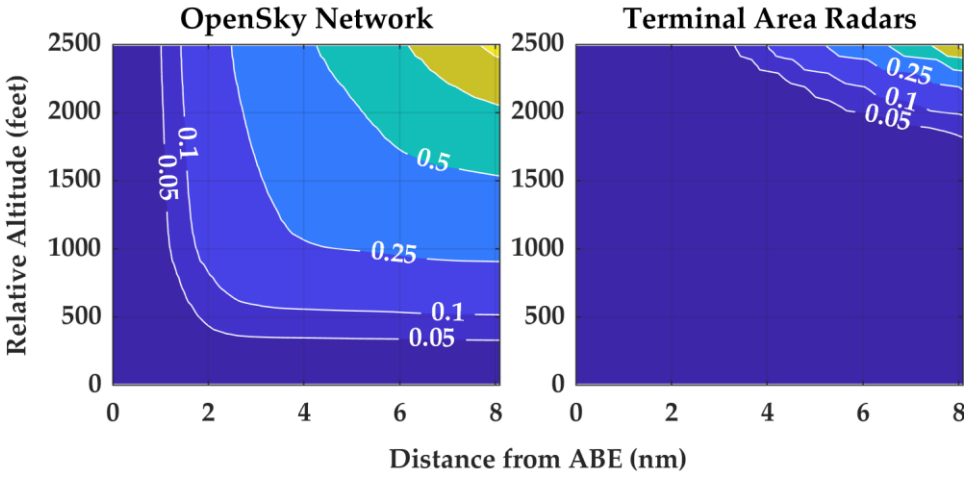

Figure 8. Fraction of aircraft positions relative to ABE.

Preprints (www.preprints.org) | NOT PEER-REVIEWED | Posted: 2 November 2021 doi:10.20944/preprints202111.0051.v1

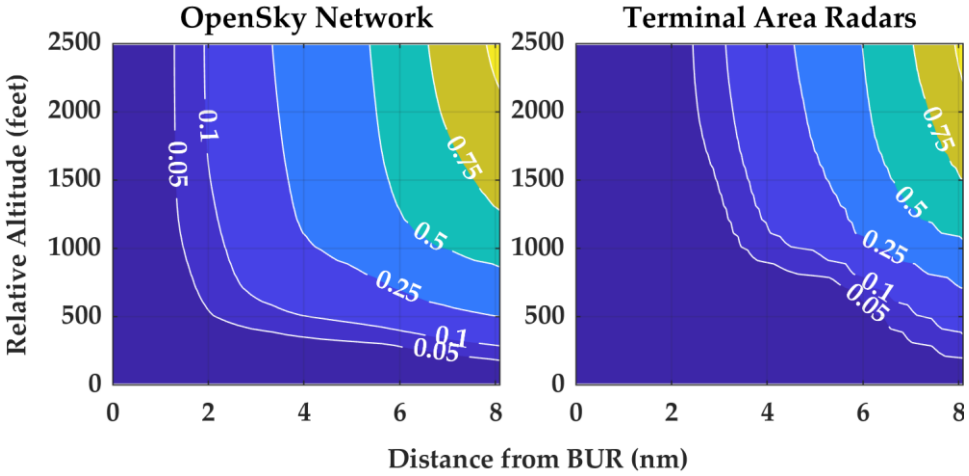

Figure 9. Fraction of aircraft positions relative to BUR.

All of the discussed biases can be observed when comparing Laurence G. Hanscom Field (BED) to Boston Logan International (BOS). BOS is located about one nautical mile from the densely populated downtown of Boston while BED is located in the less populated suburbs about 13 nautical miles away from BOS. This region is unique in that the terminal area radar, MOD, is located at BED, a Class D airport, and not BOS, the nearest Class B airport. The proceeding discussion suggests that BOS should benefit from a greater nearby population density for the OpenSky Network-based data and that BED should have a greater percentage of tracks below 500 feet for the terminal radar data due to the location of the radar. This hypothesis was supported by percent differences between BOS and BED, with BOS having 119.5% more observations for the Open Sky Network-based data and 72.3% more using terminal radar dataset. The percent difference indicates that a greater percentage of data was gained from switching the target airport of BED in the suburbs to BOS in the city. Additionally, note that for distances greater than 2.5 nautical miles with the terminal area radars, the 5% contour relative to BED is below 500 feet in Figure 10 but above 500 feet in Figure 11 relative to BOS. This indicates a greater percentage of low altitude traffic below 500 feet observed by the terminal area radars were observed closer to the radar's location at BED than away from the radar at BOS.

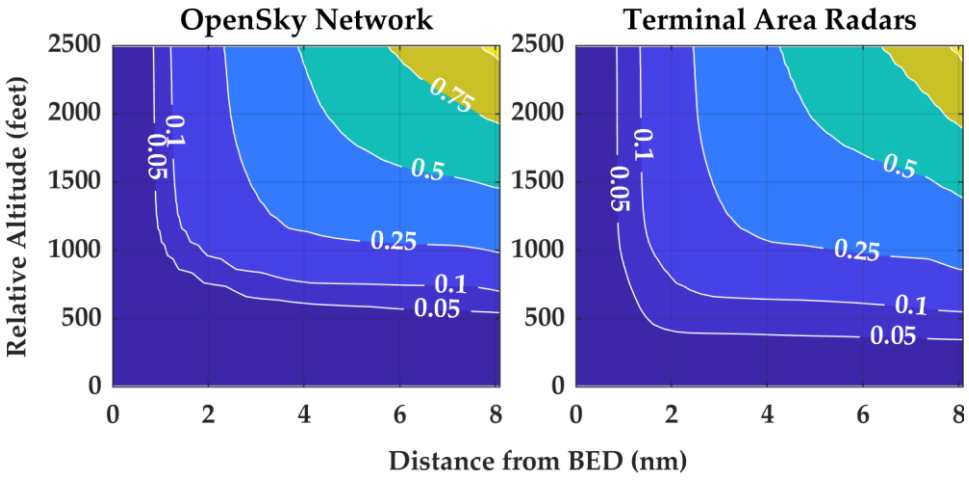

Figure 10. Fraction of aircraft positions relative to BED.

Preprints (www.preprints.org) | NOT PEER-REVIEWED | Posted: 2 November 2021 doi:10.20944/preprints202111.0051.v1

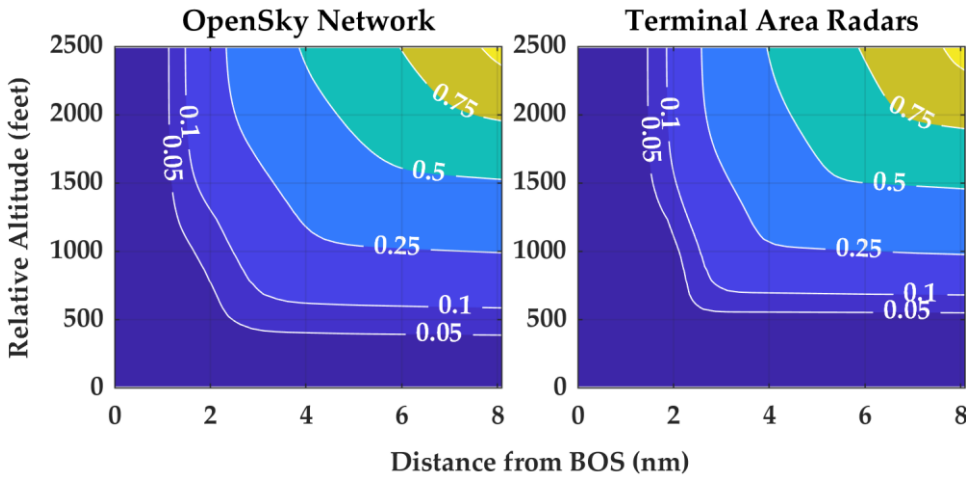

Figure 11. Fraction of aircraft positions relative to BOS.

Figures 4-11 all indicate that aircraft are rarely observed within 2 nautical miles and no more than 500 feet above airports. While the contours are dependent upon the surveillance performance of the OpenSky Network or terminal area radars (with performance likely better at higher altitudes), the general shape and conclusions drawn from the different airports are similar. The surveillance performance differs for each of the airports but drawing similar conclusions for each airport lends confidence to the analysis. Figures 1-3 also indicated that aircraft operate largely above 500 feet AGL. Assuming the contours are representative, the associated aircraft behavior aligns with many FAA regulations, such as 14 CFR § 91.119 - Minimum safe altitudes or 14 CFR § 91.129 - Operations in Class D airspace. Namely, crewed aircraft rarely should operate low and close to airports and that the majority of the time aircraft are not operating in the terminal environment. The contours could be used to estimate a quantitative bound on how often aircraft operate near airports, with an upper bound potentially of 5%.

Given our objective to identify encounters where aircraft are operating low and close to an airport, this analysis helps characterizes a challenge of meeting this objective. For model training, we're inherently seeking to identify rare events, encounter geometries that could led to a collision within a few minutes, given another rare event, a loss of separation between aircraft[36]. Accordingly, the subsequent processing steps must maximize the utility of these rare events while having a high confidence that such events transpired.

2.3. Track Intent and Runway Identification

After the initial filtering, we identified the intent for the tracks and which runway a track was interacting with when taking off or landing. Tracks are considered independently. For this processing step, there were six different intents identified. A transiting intent was indicative of a track not interacting with any runways and assumed to be transiting through the airspace. General aviation cross country flights or en route aircraft are example behaviors we sought to identify as transiting. There were two landing intents, straight and other, where straight corresponds to a straight-in landing and other is any other type of landing, such as 45 degrees, downwind, or crosswind. Similarly, there were two takeoff intents, one for straight-out and another for all other types. Finally, there was an unknown intent if a track was not assigned any of the other intents.

2.3.1. Clustering using Airport Boundaries

First, we identified if a track was operating near the airport of interest or near any airports within 10 nautical miles of the airport of interest. For each airport, an airport bounding polygon was created based on assumed airport design and traffic pattern. Assumptions based on airport design and runway approach and departure standards

 doi:10.20944/preprints202111.0051.v1

were based on the FAA Advisory Circular (AC) 150/5300-13A, Airport Design, which could differ than the approach surfaces defined in 14 CFR § 77. For generating the airport boundary, an approach and departure corridor was generated for each runway. These corridors were trapezoids (isosceles trapezium)[2], extending 2.5 nautical miles out from the runway, and 800 and 3800 feet along the narrowest and widest parallel sides. Also, the traffic pattern was estimated by a circle centered on the airport with a radius of 1.2 nautical miles. The FAA airplane flying handbook[37] states that aircraft are well clear approximately two miles away from the pattern, so the radius needed to be smaller than that. Traffic patterns are also typically defined based on the end of a runway, not the center of an airport as assumed here, but the estimated approach surfaces mitigated consequences from the simple estimation of the traffic pattern. To generate the airport boundary, a boundary was created around all the estimated approach surfaces and traffic pattern. Boundaries were not enforced to be convex.

Figure 12 illustrates the boundaries, trapezoids, traffic circles, and runways for ABE and XLL; and Figure 13 illustrates these for EWR, JRB, and LDJ. ABE and XLL each have two crossing runways in a nominal configuration. The trapezoids do not overlap and extend out in different headings. The widest parallel side of the trapezoids form part of the airport boundaries. The runway and trapezoid orientations result in the traffic pattern not influencing the shape of the airport boundary. Conversely, the traffic circles were important for the LDJ and JRB airport boundaries in Figure 13. JRB is the Downtown Manhattan heliport without a fixed runway. Without runway information, no trapezoids were calculated and the airport boundary was just the traffic circle. LDJ has a single runway, so an airport boundary for LDJ based only on the trapezoids would be narrow and just as wide as the trapezoid which would insufficiently cover the traffic pattern. However, for larger airports, like EWR, the traffic circle may barely extend past the runways and provide limited utility.

Furthermore, airport boundaries can overlap, such as EWR and LDJ. Since the model assumes intruder aircraft are not taking off or landing from nearby airports, the proximity and overlap of airport boundaries was important. This relative positioning would influence how the intent of a track was classified. After the initial spatial filtering, if a track flew through the airport boundary for any nearby airport, at any altitude, it could not be classified as taking off or landing from the airport of interest. Although this criterion was stringent, it was intended to minimize the risk of including undesired tracks landing and taking off from other airports when training the model.

[2] Trapezoid shape based on dimensions B, C, D from Figure 3-2 and Table 3-2 from AC 150/5300-13A.

Preprints (www.preprints.org) | NOT PEER-REVIEWED | Posted: 2 November 2021 doi:10.20944/preprints202111.0051.v1

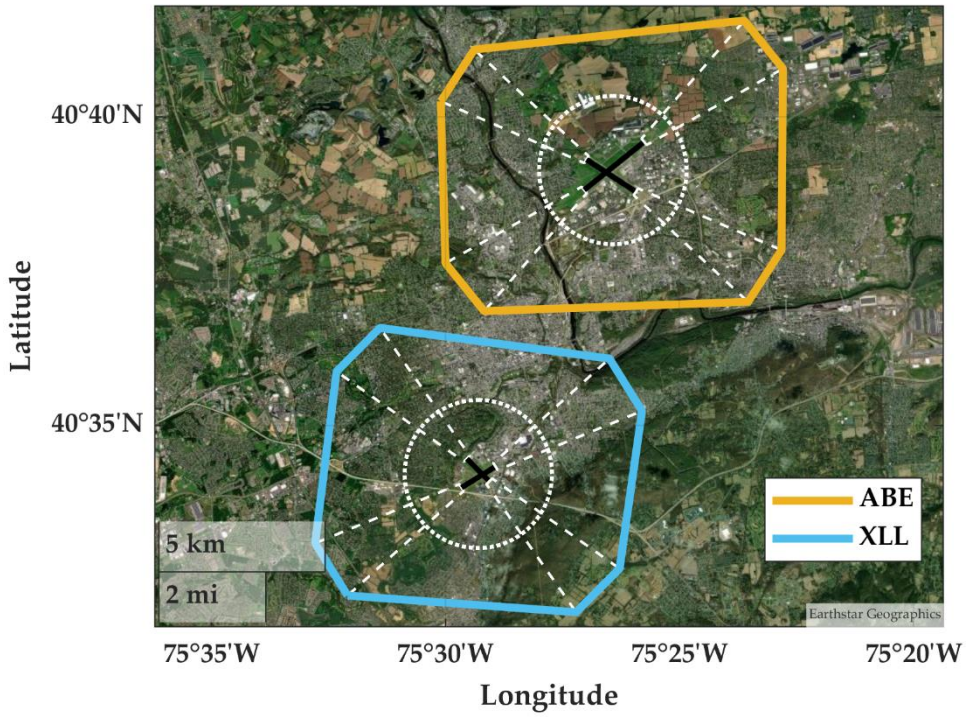

Figure 12. Airport boundaries for ABE and XLL. Runways are colored in black and the approach trapezoids and traffic circles are colored in white.

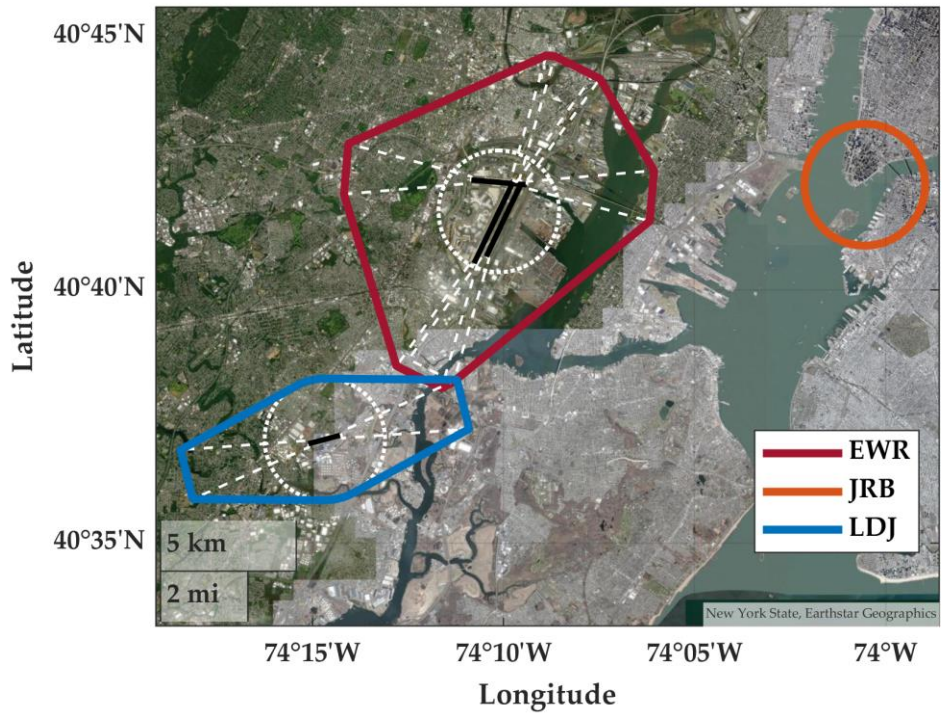

Figure 13. Airport boundaries for EWR, JRB, and LDJ. Runways are colored in black and the approach trapezoids and traffic circles are colored in white.

Preprints (www.preprints.org) | NOT PEER-REVIEWED | Posted: 2 November 2021 doi:10.20944/preprints202111.0051.v1

2.3.2. Clustering using Runway Corridors

Next, if a track was within the airport boundary for only the airport of interest, we determined if the track was also within the runway two-dimensional approach and departure corridor. These corridors were similar to the trapezoids used to generate the airport boundary but also extended 8 nautical miles from each runway[3]. A track must be in a runway's corridor for at least 30 seconds. Each runway corridor was assessed independently and a track could be assigned multiple runways. Figures 14 illustrate these corridors for ABE. Observe how the XLL airport boundary intersects with one of the ABE runway corridors. Given the requirement that a track can only intersect the airport boundary for the airport of interest, ABE in Figure 14, the majority of the tracks in the overlapping could not considered as taking off or landing from ABE.

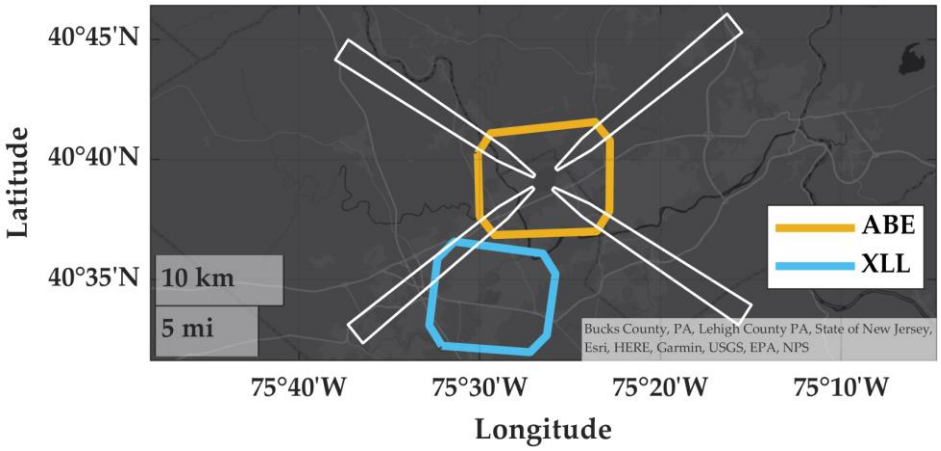

Figure 14. Runway corridors for ABE with airports boundaries for ABE and XLL.

2.3.3. Vertical Rate, Altitude, and Relative Heading

If a track segment satisfied the spatial and temporal requirements based on the runway corridor, it was furthered assessed based on vertical rate, altitude, and the relative distance from the runway. If these additional criteria were met, the track was classified as either taking off or landing. The vertical rate of the track when it was in the corridor was assessed to help determine if a track was taking off or landing. The vertical rate had magnitude and duration components. When in a corridor, the magnitude of the vertical rate had to be at least 300 feet per minute for a specific duration. This threshold duration could either be the time to vertically transit from the minimum and maximum track altitudes or 30% of the entire duration the track is in a corridor. These criteria also were iterated upon between version 3.0 and 2.0 of the models. It was initially 50% and 500 feet per minute but the initial criteria excluded tracks with many points in the corridors or with slower vertical rates near a runway. If the vertical rate was negative and the track decreased altitude, it was classified as landing; and vice versa for takeoffs.

To be classified as taking off or landing, when in a corridor the track must fly within 2.5 nautical miles and 750 feet from the end of the runway of interest. This lateral and vertical criterion corresponds to the aviation heuristic 1 in 60 rule and an assumed 3 degree glide slope. This criterion was notably iterated on during model development. For version 2.0 of the model, the criterion was not based on an assumed 3 degree glide slope and was instead, 1 nautical mile and 475 feet. Version 1.0 of the model also did not con-

[3] Shape based on dimensions B, C, D, E from Figure 3-2 and Table 3-2 from AC 150/5300-13A.

Preprints (www.preprints.org) | NOT PEER-REVIEWED | Posted: 2 November 2021 doi:10.20944/preprints202111.0051.v1

sider a nominal glide slide. It employed an altitude ceiling of 1500 feet relative to the runway and a single point must be within 4000 feet laterally of the runway.

Finally, to determine if the takeoff was straight-out or the landing was straight-in, we calculated the magnitude heading relative to the runway for all track points in the corridor. If the 95th percentile of all relative headings was 30 degrees or less, the track was classified with an intent of either straight landing or take off. Otherwise it was classified as a non-straight landing or takeoff. For straight takeoff and landings, any points immediately before or after the track enters or exits the corridor that satisfied a 40 degree relative heading threshold were also assigned a straight landing or take off intent. For subsequent processing steps, only the straight maneuvers would be considered for the ownship.

For the other intents, a change in altitude criteria was used to classify points outside of a corridor. For takeoffs, after exiting the corridor, points until the maximum altitude was achieved were as labeled as with the takeoff intent. Conversely points descending from the maximum altitude prior to entering the corridor were labeled with a landing intent. For example, Figure 15 illustrates the filtered straight-in and other landing tracks for an ABE runway.

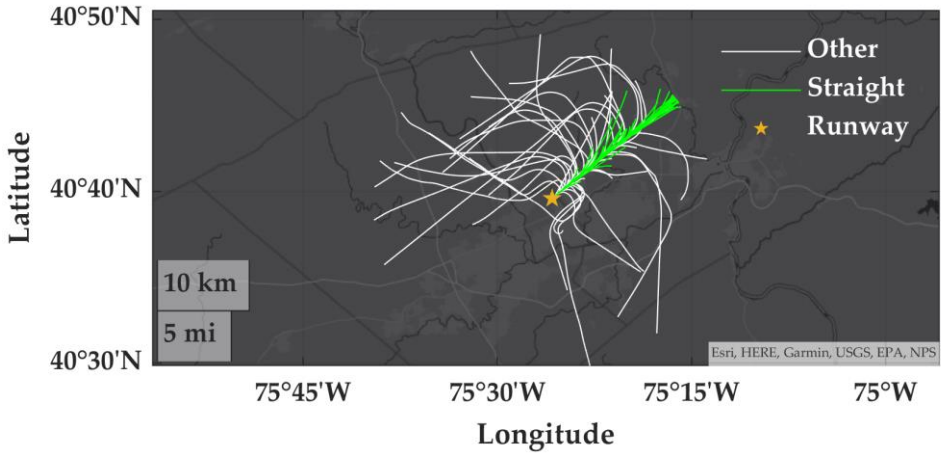

Figure 15. Landing at ABE using the OpenSky Network-based aerodromes dataset.

Version 1.0 and 2.0 calculated relative heading differently. Instead of calculating the relative heading for all points in a corridor, previous versions only considered the relative heading at two locations: the first and last points within the corridor. The corridors were also not based on approach surfaces but rectangular bounding boxes extended from each runway.

2.3.4. Transiting Aircraft

If the minimum altitude for all points within a corridor was greater than 1500 feet relative to the runway and the maximum altitude was less than 5000 feet, then the track would be labeled with an intent of transit. If a track intersected any airport boundary but none of the corridors, the same altitude criteria would applied to determine if the track was transiting over the airport. For example, any tracks that intersected solely the XLL boundary would need a minimum altitude of 1500 feet to be classified as transiting. This criterion was successful in filtering out low altitude traffic operating from nearby airports, while not filtering en route traffic flying above the airport. Figure 16 illustrate transiting aircraft for ABE and Figure 17 illustrates the notional condition if the altitude criteria were changed from 1500 to 0 feet relative to ABE. Note the lack of low altitude tracks colored blue within the centered ABE boundary in Figure 16 but the presence of low altitude tracks in Figure 17. This difference illustrates tracks established in the traffic pattern around ABE that satisfied the airport boundary but failed to satisfied the runway corridors criteria. Also evident was the low altitude traffic operating near XLL that was southwest from ABE and filtered out in Figure 16.

Preprints (www.preprints.org) | NOT PEER-REVIEWED | Posted: 2 November 2021 doi:10.20944/preprints202111.0051.v1

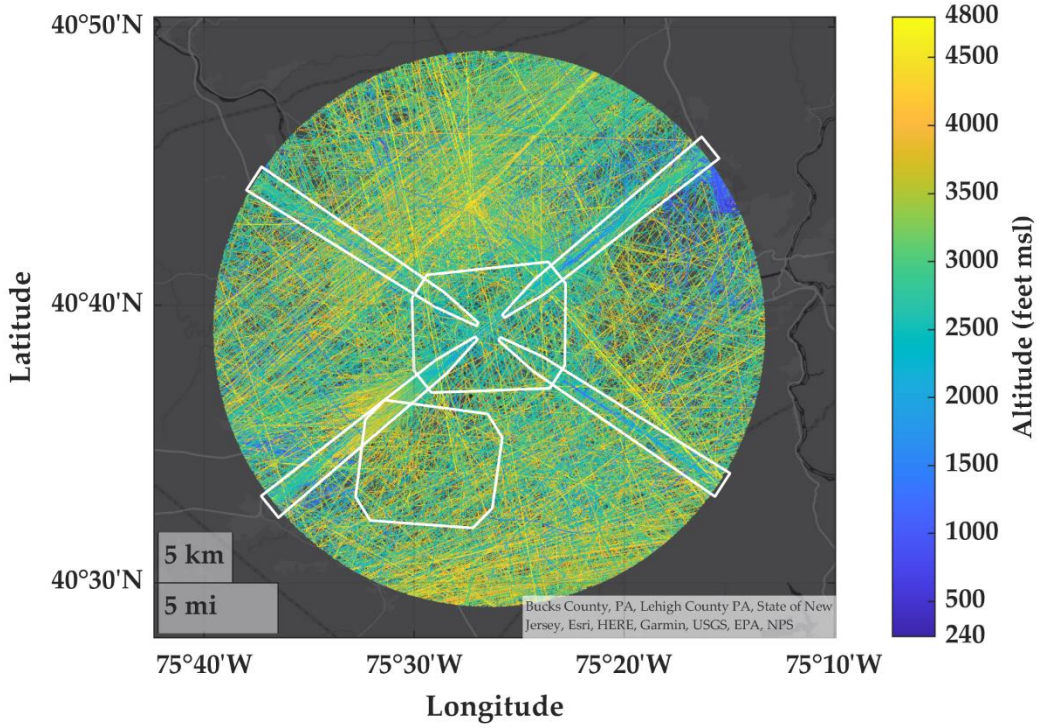

Figure 16. Transiting tracks for ABE overlaid with runway corridors for ABE and airport boundaries for ABE and XLL. The minimum transiting altitude was 1500 feet relative to ABE. This altitude limit was used for model training. Tracks sourced from the OpenSky Network-based aerodromes dataset.

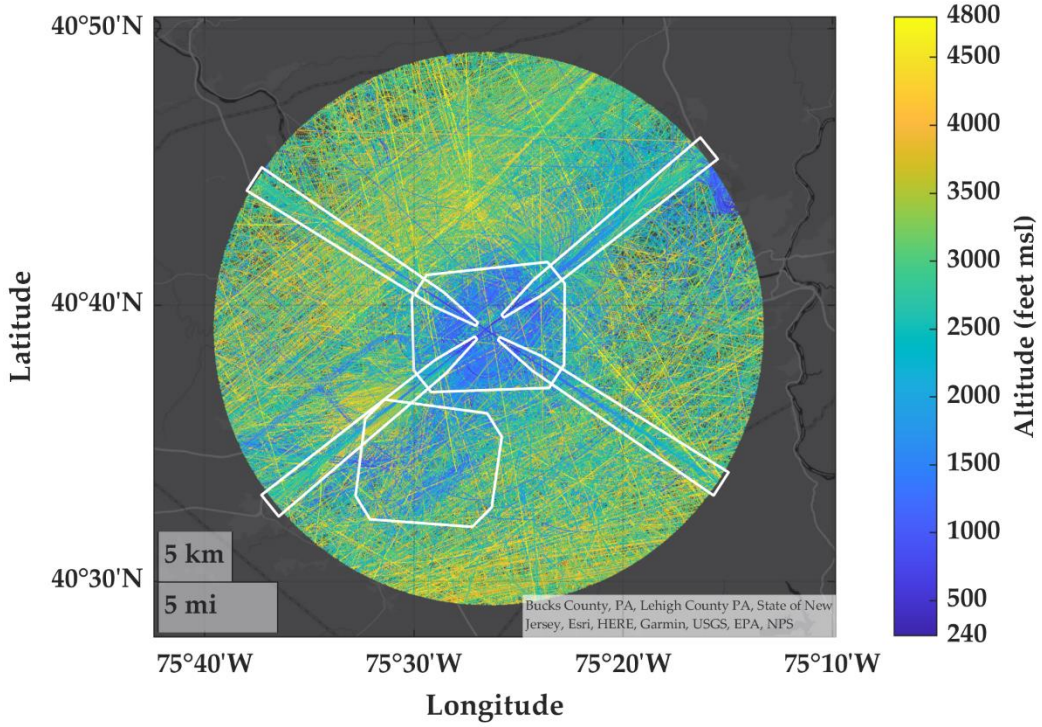

Figure 17. Transiting tracks for ABE overlaid with runway corridors for ABE and airport boundaries for ABE and XLL. The minimum transiting altitude was 0 feet relative to ABE. This altitude criteria and figure is illustrative and not used for model training. Tracks sourced from the OpenSky Network-based aerodromes dataset.

Preprints (www.preprints.org) | NOT PEER-REVIEWED | Posted: 2 November 2021 doi:10.20944/preprints202111.0051.v1

2.4. Encounter Identification

The previous step only identified the intent (e.g. landing, taking off, transiting) of independent tracks, the next step was to identify pairs of tracks that encountered each other. First, we identified pairs of tracks where one aircraft must have an intent of a straight-in landing or straight-out takeoff. Next, for the pairs of tracks, we determined if there was at least one second overlap in UTC time. After assessing intent and time, there could had been tens to hundreds of thousands of potential encounters, at least one second in duration, that needed to be further assessed. Subsequently, we calculated which pairs had at least thirty seconds of overlap and for these also calculated the horizontal and vertical separation between the pairs of aircraft when they overlapped in time. If the tracks at any point were separated 4 nautical miles or less laterally and 2000 feet or less vertically, the pair was designated as an encounter. Both separation criteria had to be satisfied such that an encounter must be at least 30 seconds in duration when both aircraft tracks exist. Satisfying all these criteria was challenging and an overwhelmingly majority of pairs that had any overlap in time were rejected due to the spatial criteria.

2.4.1. Example Training Encounters

Figures 18-20 illustrate three example encounters identified for ABE using the OpenSky Network-based aerodromes dataset. Figure 18 illustrates an encounter where both aircraft are landing at the same runway. While versions 1.0 and 2.0 did not include airports with multiple runways, this encounter is representative of the data used to train the preliminary models. Particularly, this encounter highlights the RTCA SC-228 imposed constraints on the aircraft. While both aircraft are landing, the final approach and landing for the intruder can be highly variable across encounters, whereas ownship must always have a minor relative heading difference from the runway. Figure 19 also highlights this but for an example where the intruder is taking off from a different runway. Lastly, Figure 20 demonstrates that ownship may exhibit some minor turning behavior due to the relative heading threshold of 30 degrees or less. Also exhibited is that aircraft, particularly intruders, can be oriented many nautical miles away from the runway. Specifically, in Figure 20, the nearest the intruder was to the runway was about 5.2 nautical miles with a portion of the track not in Class C airspace.

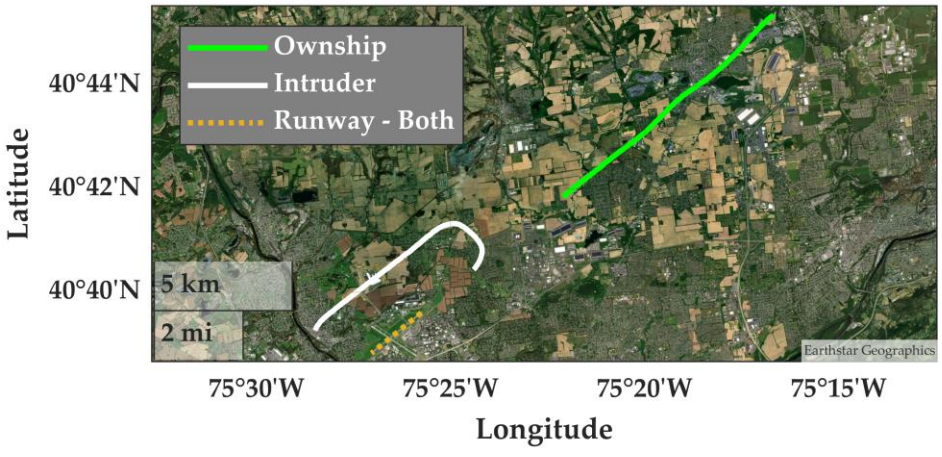

Figure 18. Example identified encounters at ABE. Both aircraft were landing at the same runway. The encounter had a duration of 222 seconds.

Preprints (www.preprints.org) | NOT PEER-REVIEWED | Posted: 2 November 2021 doi:10.20944/preprints202111.0051.v1

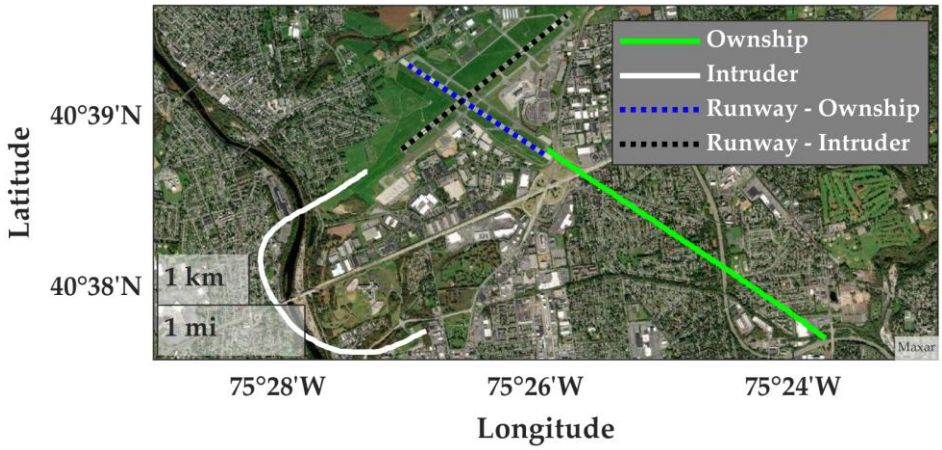

Figure 19. Example identified encounter at ABE. Ownship was landing and the intruder was taking off from a crossing runway. The encounter had a duration of 94 seconds.

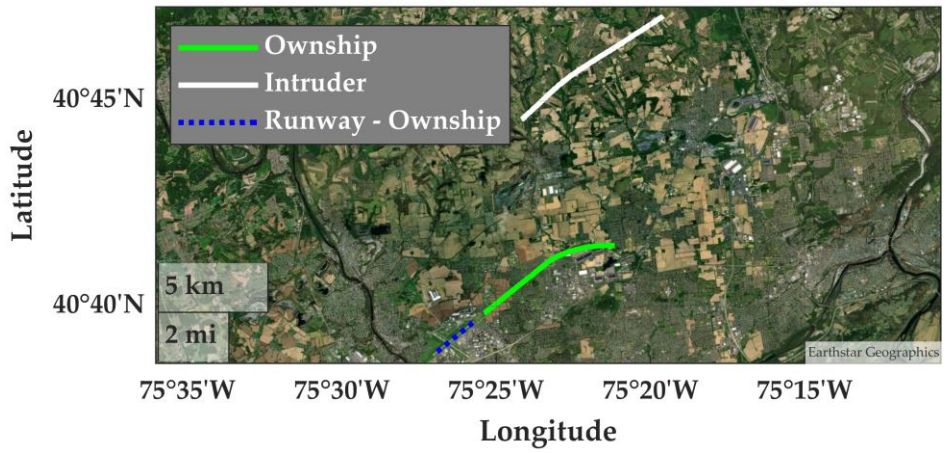

Figure 20. Example identified encounter at ABE. Ownship was landing and the intruder was transiting through the airspace. The encounter had a duration of 139 seconds.

2.4.2. Encounter Quantities

Table 3 summarizes how the data was filtered from the initial spatial filtering to the final set of identified encounters for three representative airports.

Table 3. Processing summary when using the OpenSky Network aerodromes dataset.

Count	ABE	ADS	LBJ
Points after initial spatial filtering	1,816,670	20,954,315	14,538,290
Takeoffs or landings (any)	877	2,913	3
Transiting intruders	4,522	38,917	71,881
Potential encounters based on intent and time	28,174	753,067	23,889
Final identified encounters for training	22	402	0

While we had significantly less data for ABE than LBJ, ABE had more potential encounters that satisfied the intent criteria for potential encounters and had more encounters identified. This was attributed to the differences of the airspace and design of airports near ABE or LBJ. In particular, the immediate proximity of LBJ to the larger EWR (Figure 13) resulted in the majority of the tracks filtered out for consideration as ownship. Furthermore, the majority of traffic was likely operating from or to EWR, so the large quantity of data was more reflective of EWR than the smaller LBJ. Similarly, as discussed

Preprints (www.preprints.org) | NOT PEER-REVIEWED | Posted: 2 November 2021 doi:10.20944/preprints202111.0051.v1

in Section 2.2, we observed significantly more traffic near ADS due the greater population density of the Dallas Fort Worth metroplex and increased traffic around the Class B airports of DFW and DAL. While ABE had less than a tenth of the data as ADS, more potential ownship tracks were identified per observation points for ABE than ADS.

2.4.3. Encounter Duration

For all airspace classes when using the aerodromes dataset, the median duration of identified encounters for model training was at least 87 seconds and 10% or fewer encounters had a duration of 39 seconds or less. The median was at least 100 seconds when using the terminal area radars dataset. These two statistics indicate that the requirement for an encounter to be at least 30 seconds was not overly burdensome and not a significant factor when rejecting an encounter for model training. If the duration requirement increased to 60 seconds when using the aerodromes dataset, about a third of the current Class D and other encounters would be rejected, while only 15% of Class C encounters would be rejected. Comparably, about a quarter of the current Class D and Other encounters and a smaller percentage of Class C encounters would be rejected when using the terminal area radars dataset.

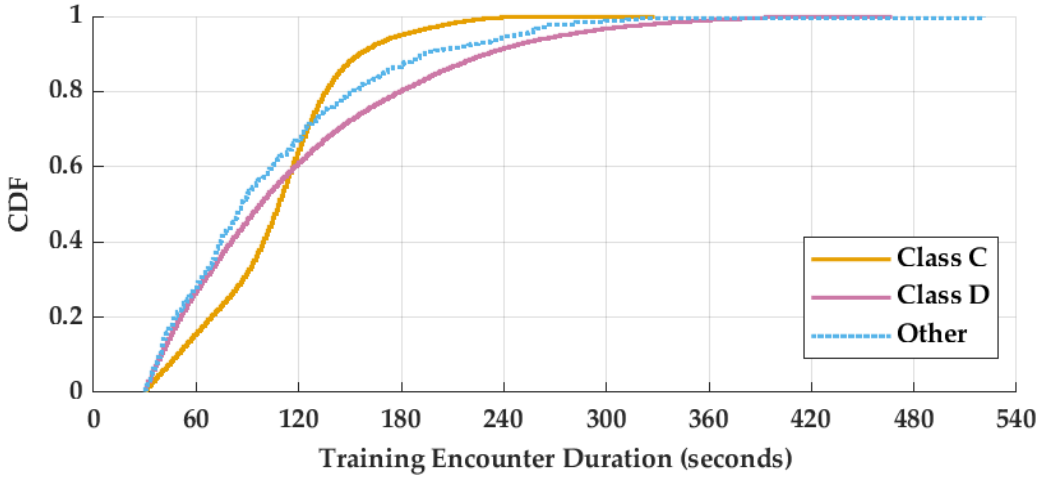

Figure 21. Distribution for duration of encounters identified using the OpenSky Network-based aerodromes dataset. For all airspace classes, the median duration was at least 87 seconds.

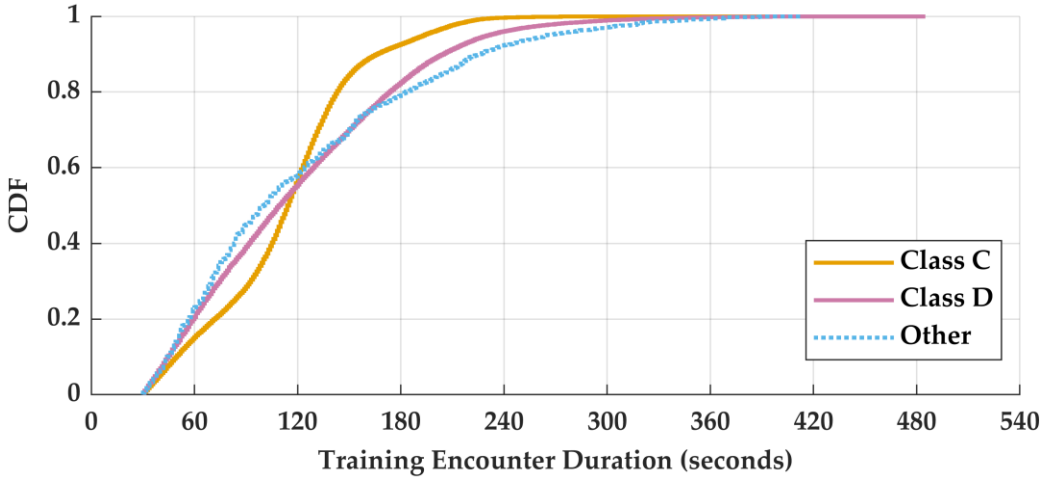

Figure 22. Distribution for duration of encounters identified using the terminal area radars dataset. For all airspace classes, the median duration was at least 100 seconds.

Preprints (www.preprints.org) | NOT PEER-REVIEWED | Posted: 2 November 2021 doi:10.20944/preprints202111.0051.v1

While the duration of training encounters had a minimal dependence on airspace class or dataset, the quantity of encounters identified for each airport of interest was biased towards a small percentage of airports. Table 4 reports the distribution of how many encounters were identified for an airport. For example, Table 4 reports that no encounters were identified for 29 Class C airports and that at least 100 encounters were identified at 24 Class C airports when using the OpenSky Network-based aerodromes dataset.

94% of the Class E or G (Other) airports when using the OpenSky Network-based aerodromes dataset and 89% of other airports with the terminal area radar dataset had no encounters identified. For the terminal area radars dataset, 48% of encounters in Other airspace were identified from 1% of the airports (n = 4) with any data after the initial spatial filtering. However, the surveillance coverage at low altitudes near an airport's surface was highly variable and why the initial spatial filtering (Section 2.2) was designed to reduce the computational burden for track classification and encounter identification rather than designed to identify encounters upfront.

Table 4. Airport count with quantity of training encounters.

Airspace Class	Dataset	0	(0,10)	[10, 100)	[100, ∞)	Total
C	Aerodromes	29	9	12	24	74
C	Terminal Radars	5	0	2	9	16
D	Aerodromes	139	40	45	44	268
D	Terminal Radars	43	6	25	44	118
Other	Aerodromes	829	37	13	0	879
Other	Terminal Radars	371	24	19	4	418

2.5. Model Training and Structure

With encounters identified, the statistical models could now be trained. The terminal model consisted of an encounter geometry model and a trajectory propagation model. The first component, the encounter geometry model, describes the geometrical conditions of two encounter aircraft at their point of closest approach. The second component, the trajectory generation model, then describes the flight path for each aircraft leading to and continuing from their point of closest approach. Like the RADES-based correlated model, this was a generic model with no dependency on geography or locations.

While the trained model was used subsequently in simulations where ownship was assumed to be an UAS, the model itself was trained assuming that all encounters identified in Section 2.4 consisted of traditional crewed aircraft. Section 2.6 describes how the trained model was sampled to enforce this UAS assumption.

2.5.1. Relative Local Coordinate System

Encounters are described in a coordinate system where all altitudes are relative to the mean runway elevation. Angular units are represented on a standard polar grid increasing in counterclockwise orientation. When training the model, the aircraft trajectories are rotated using a two-dimensional rotation matrix such that the runway the ownship is using lays directly on the y-axis, with the runway mean position located at (0,0). The runway is assumed to be a single point, rather than a vector or polygon. When training the model, positions and distances are relative to the mean runway position for the airport of interest. Since we trained a generalized model, this is a potential source of bias and error, as the mean runway position will vary for different airports.

Also, the runway is oriented above ownship on the y-axis: that is, ownship has a relative angular position (bearing) with a range of [180, 360] degrees. When projected onto a Cartesian coordinate system, the y-axis is oriented from 270 to 90 degrees, and x-axis from 180 to 0 degrees.

Figure 23 illustrates the bearing distribution for the ownship forward trajectory model, with similar distributions within the ownship backwards trajectory model. As bearing is a relative position, the distribution given a landing or takeoff intent are similar.

Preprints (www.preprints.org) | NOT PEER-REVIEWED | Posted: 2 November 2021 doi:10.20944/preprints202111.0051.v1

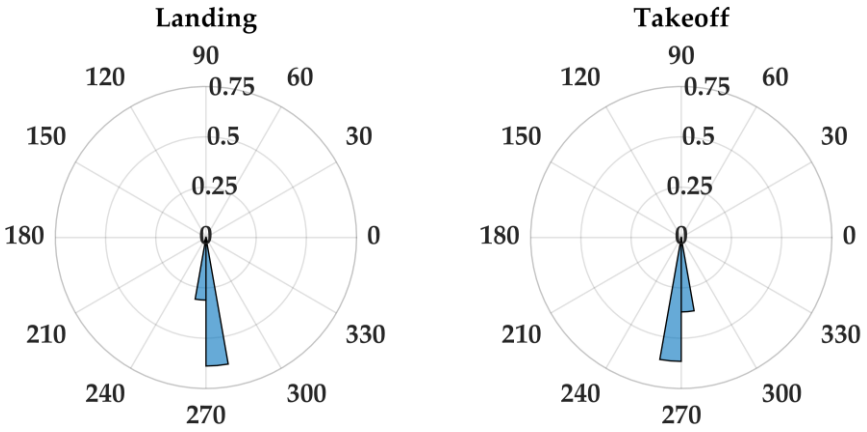

Figure 23. Bearing (angular position) distribution of the ownship forward trajectory model. Bin widths are 10 degrees.

Bearing is the angular position, whereas heading is the correspondingly angular vector, that is the direction of flight. Figure 24 illustrates the heading distribution for the ownship forward trajectory model. Unlike the bearing distribution in Figure 23, the heading distribution is dependent upon whether ownship is taking off or landing. When landing, the average heading is 90 degrees, as the ownship is flying along the negative y-axis towards the mean runway position at (0,0); whereas when taking off, the ownship is flying away from the runway such that the mean heading is 270 degrees. The heading and bearing also reflect that ownship takeoffs and landing were constrained to be straight-out or straight-in; the distribution for the intruder models are different with the distribution over a wider range of values.

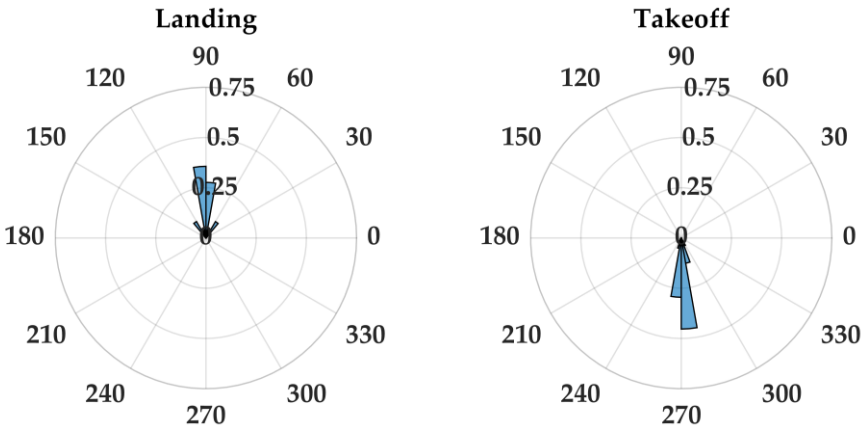

Figure 24. Heading (angular vector) distribution of the ownship forward trajectory model. Bin widths are 10 degrees.

The differences with the intruder distributions is best illustrated by Figure 25 with the bearing and heading distributions of the intruder forward trajectory model given that the intruder is transiting through the airspace. Compared to the more constrained ownship distributions, the intruder distribution has a wider distribution over bearing and a significantly more encompassing distribution over the full 360 degree range of headings. The intruder bearing distribution is reflective of the encounter separation criteria. Since ownship predominantly has a bearing in the range of [260, 280] degrees and encounters occur when aircraft are close to each other, it is not surprising that the intruder has a similar mean bearing. However, since transiting intruders are not flying to or from the

Preprints (www.preprints.org) | NOT PEER-REVIEWED | Posted: 2 November 2021 doi:10.20944/preprints202111.0051.v1

mean runway position at (0,0), they operate more liberally throughout the airspace, as represented by the more diverse heading distribution. Note that Figure 25 is not dependent upon ownship intent and we do not observe an equal quantity of ownship landings and takeoffs.

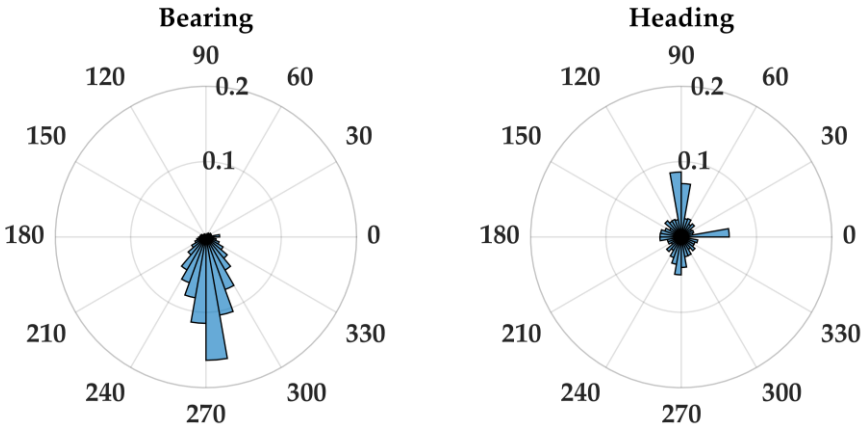

Figure 25. Bearing and heading distributions for the intruder forward trajectory model given an intruder intent of transiting through the airspace. Bin widths are 10 degrees.

2.5.2. Encounter Geometry Model

The encounter geometry model describes the position, speed, and direction of two aircraft at their horizontal closest approach. Some variables were smoothed using a locally weight temporal smoother with a Gaussian kernel. It uses the following variables:

- Airspace class: Airspace class of the airport.
- Ownship intent: The intent of the ownship, per Section 2.3, of either a straight landing or take off.
- Intruder intent: The intent of the intruder, per Section 2.3, of either landing, taking off, or transiting. Unlike the ownship, the intruder's intent is not assumed to be straight.
- Intruder type: The type of aircraft of the intruder: can either be fixed-wing or rotorcraft. Note that while the OpenSky Network-based uncorrelated models are individually organized by aircraft type[12], aircraft type is an explicit model variable here.
- Intruder runway: The runway the intruder was leveraging relative to the ownship. Designated as "same" if both aircraft were operating from the same runway; parallel" if the intruder was operating from a runway that did not intersect the ownship's runway; as "crossing" if the intruder was operating from an runway that intersected the ownship's runway; and "none" if the intruder intent was transiting.
- Ownship distance from runway: The horizontal distance between the ownship position at CPA and the runway mean position;
- Ownship bearing from runway: The polar angle of the ownship's position at CPA ;
- Ownship altitude: The altitude of the ownship relative to the runway elevation at CPA;
- Ownship speed: The smoothed speed of the ownship at CPA as estimated by a finite difference of the trajectory position data;
- Ownship heading: The direction of flight of the ownship at CPA ;
- Intruder distance from runway: The horizontal distance between the intruder position at CPA and the runway mean position
- Intruder bearing from runway: The polar angle of the intruder's position at CPA;
- Intruder altitude: The altitude of the intruder relative to the runway elevation at CPA;

Preprints (www.preprints.org) | NOT PEER-REVIEWED | Posted: 2 November 2021 doi:10.20944/preprints202111.0051.v1

- Intruder speed: The smoothed speed of the intruder at CPA as estimated by a finite difference of the trajectory position data;
- Intruder heading: The direction of flight of the intruder at CPA.

Some of these variables were more constrained in versions 1.0 and 2.0. The initial model constrained ownship intent to just landing, intruder intent could not be transiting, and the intruder runway was always the same as the ownship. Version 2.0 introduced taking off ownships and transiting intruders, but the same runway assumption was still enforced. Version 3.0 expanded intruder runway to the four options while also improving the assumptions about transiting intruders when other airports were nearby (Section 2.3.4).

These variables were associated via a graphical model that indicates dependency relationships. In this graph, the variables are nodes and the dependencies are directed edges. Thus, in Figure 26 below, the intruder's track is dependent on its distance and its bearing from the runway. Those variables in turn are dependent on several other variables. There are numerous ways the variables could be connected, but at this stage the graph has been structured based on engineering judgement. Future work could optimize the graph structure to best characterize the data with the fewest connections. The dependencies in this model are conditional probabilities, so the graph can be referred to as a Bayesian network.

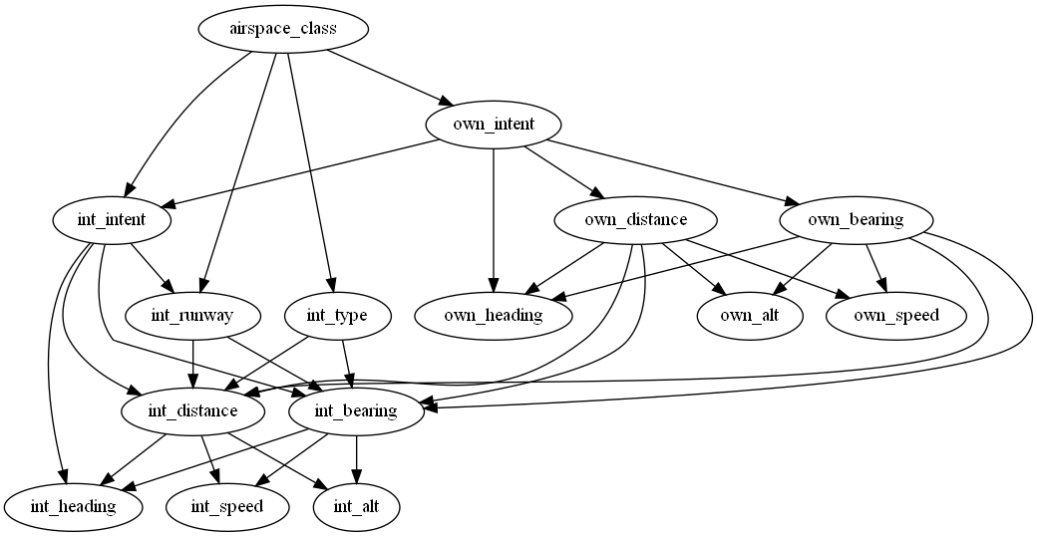

Figure 26. Bayesian network for the encounter geometry model.

Some variables, as identified in Table 5 below, are inherently discrete. Other variables, identified in the Table 6 below, are inherently continuous. For representation in this model, the continuous values in the observed data must be discretized during training per the cutpoints identified in the table. Sampling the model yields discrete values for these variables, with a continuous value subsequently sampled from the bin with a uniform distribution.

Table 5. Encounter geometry model discrete variables.

Variable	Node Label	Values
Airspace Class	class	[1 – B, 2 – C, 3 – D, 4 – Other]
Ownship Intent	Ownship_intent	[1 – Land, 2 – Takeoff]
Intruder Intent	int_intent	[1 – Land, 2 – Takeoff, 3 – Transit]
Intruder Type	int_type	[1 – Fixed-Wing, 2 – Rotorcraft]
Intruder Runway	int_runway	[1 – Same, 2 – Parallel, 3 – Cross-

Preprints (www.preprints.org) | NOT PEER-REVIEWED | Posted: 2 November 2021 doi:10.20944/preprints202111.0051.v1

	ing, 4 – None (Transit)]

Table 6. Encounter geometry model continuous variables.

Variable (Units)	Node Label	Cutpoints
Ownship Altitude (feet)	own_alt	[200, 500, 1000, …, 3000, 5000]
Ownship Bearing (degrees)	own_bearing	[0, 15, 30, …, 165, 175, 185, 195, 210, 225, …, 360]
Ownship Distance (nautical miles)	own_distance	[0, 0.5, 1, 2, 3, 4, 5, 8]
Ownship Speed (feet per second)	own_speed	[75, 150, 225, 300, 375, 450]
Ownship Track (degrees)	own_trk_angle	[-180, -175, -165, …, 175, 180]
Intruder Altitude (feet)	int_alt	[200, 500, 1000, …, 3000, 5000]
Intruder Bearing (degrees)	int_bearing	[0, 15, 30, …, 165, 175, 185, 195, 210, 225, …, 360]
Intruder Distance (nautical miles)	int_distance	[0, 0.5, 1, 2, 3, 4, 5, 8]
Intruder Speed (feet per second)	int_speed	[75, 150, 225, 300, 375, 450]
Intruder Track (degrees)	int_trk_angle	[-180, -175, -165, …, 175, 180]

2.5.3. Trajectory Propagation Model

The trajectory generation models describe how the position of the two encountering aircraft evolves before and after their closest point of approach (CPA). It is important to note that the ownship and intruder models are trained separately. While the encounter generation model considered the relatively geometry between aircraft, the trajectory propagation models assumed track independence. The training data for this model were the independent sets of ownship and intruder tracks from identified encounters. Figure 24 highlights this by visualizing all the ownship and intruder tracks for ABE used as training data for the trajectory propagation models; while Section 2.4.1 depicted specific encounters included in the set of tracks visualized by Figure 27. Once again, note the limited behavior and diversity of ownship tracks due to the RTCA SC-228 imposed constraints of limiting ownship to straight takeoff and landings.

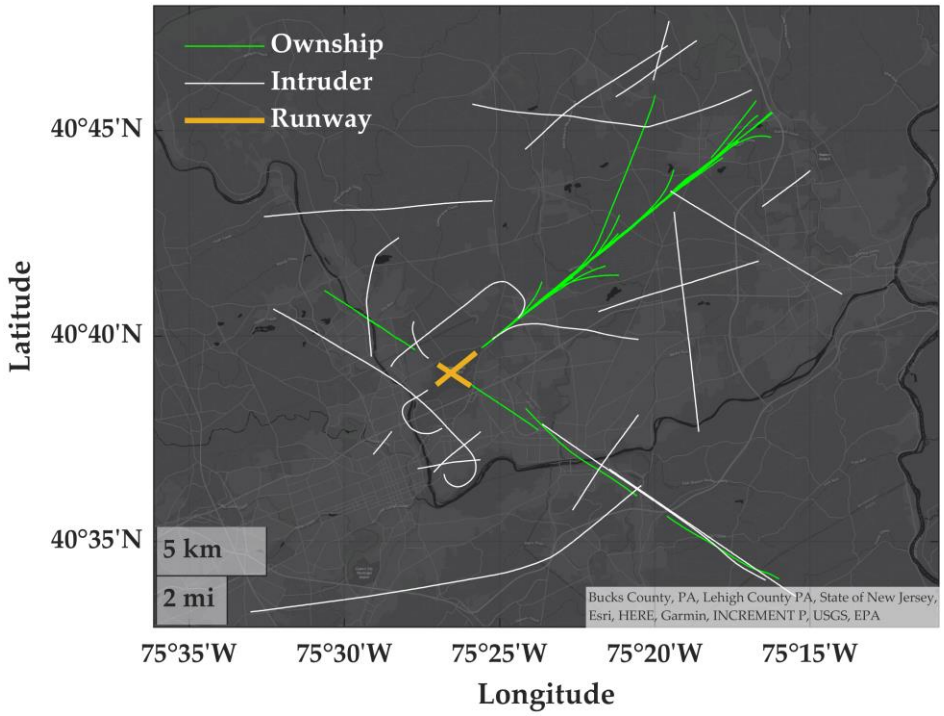

Figure 27. Example ownship and intruder tracks near ABE used for model training.

Preprints (www.preprints.org) | NOT PEER-REVIEWED | Posted: 2 November 2021 doi:10.20944/preprints202111.0051.v1

The ownship and intruder trajectory propagation models have a similar model structure with a difference in the temporal variables. The forward propagation models transition from time (t) to (t+1) after CPA has occurred, while the backwards propagation model is for time (t) to (t-1) prior to CPA. Specifically, they use the following variables:

- Intent: The aircraft's intent, same as defined for the encounter geometry model.
- Distance from runway: The horizontal distance between the aircraft position and the runway mean position over time;
- Bearing angle from runway: The polar angle of the aircraft's position;
- Heading angle: The direction of flight of the aircraft;
- Altitude: The altitude of the aircraft relative to the runway elevation over time.
- Speed: The smoothed speed of the aircraft over time as estimated by a finite difference of the trajectory position.

As with the encounter geometry model, the relationships between variables are represented as a graph. Here, time dependencies are introduced into the graph as well. As illustrated in Figure 28 below, the aircraft's track at the next time step is dependent on its current track, its bearing from the runway, and its distance from the runway. These dependencies are relied on to emulate, e.g., an intruder flying a traffic pattern: as the aircraft flies downwind, the likelihood increases that it will make a turn onto the base leg. The strength of that likelihood is learned from the observed trajectory data. Since the dependencies in the model are conditional probabilities, the graph forms a Bayesian network. In this case, since it incorporates time dependencies, it is referred to as a Dynamic Bayesian network. Note that the bearing and distance variables change over time when sampling the model, but those changes must be computed after sampling for the heading and speed at each time step. This model structure was based on the Dynamic Bayesian network of the uncorrelated encounter models, which did not model distance or bearing with respect to some spatial point.

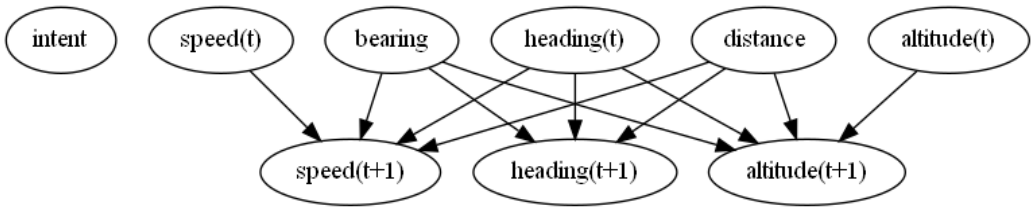

Figure 28. Dynamic Bayesian network for the trajectory forwards propagation model.

All of the variables in the trajectory generation model, defined in Table 7, are inherently continuous. Note that some cutpoints are different from those for the same variable in the encounter geometry model (e.g., altitude is more finely discretized here). For a given training dataset, different forward and backwards propagation models are trained for each intent of landing, taking off, and transiting. Forwards propagation models are trained on time-ordered trajectory data while backwards propagation models use reverse-time-ordered trajectory data for training. Future work may consolidate some or all of these separate models.

Table 7. Trajectory generation model continuous variables.

Variable (Units)	Node Label	Cutpoints
Intent	intent	[1 – Land, 2 – Takeoff, 3 – Transit]
Distance (nautical miles)	distance	[0, 0.5, 1, 2, 3, 4, 5, 8]
Bearing (degrees)	bearing	[0, 5, 15, 25, …, 355, 360]
Altitude (feet)	altitude	[200, 300, …, 2000, 2500, 3000, 5000]
Speed (feet per second)	speed	[75, 100, 150, 200, …, 350, 450]
Track (degrees)	trk_angle	[-180, -175, -165, …, 175, 180]

Preprints (www.preprints.org) | NOT PEER-REVIEWED | Posted: 2 November 2021 doi:10.20944/preprints202111.0051.v1

2.6. Model Sampling and Encounter Generation

Once the model has been trained with the observed trajectory data, it can be sampled to generate new encounters ("synthetic encounters") representative of observed behavior. Encounter generation is completed in three steps: sampling the geometry model, sampling the trajectory models, and rejecting or accepting the encounter based on criteria derived from assumptions when training the model.

2.6.1. Sampling the Encounter Geometry Model

First the encounter geometry is sampled to identify the geometry at CPA. The encounter geometry model is sampled with a uniform prior (i.e., absent any additional information, that all combinations of variables are equally likely). Since this model is not a Dynamic Bayesian network with a transition model, sampling is a one step process. The model samples describe the aircraft positions at CPA given distance and bearing relative to a runway's mean position. We translate this into a local Cartesian coordinate system where the runway mean position is at (0,0). Figures 29 and 30 illustrate 500 samples from the geometry model where ownship is taking off and the intruder is landing or transiting.

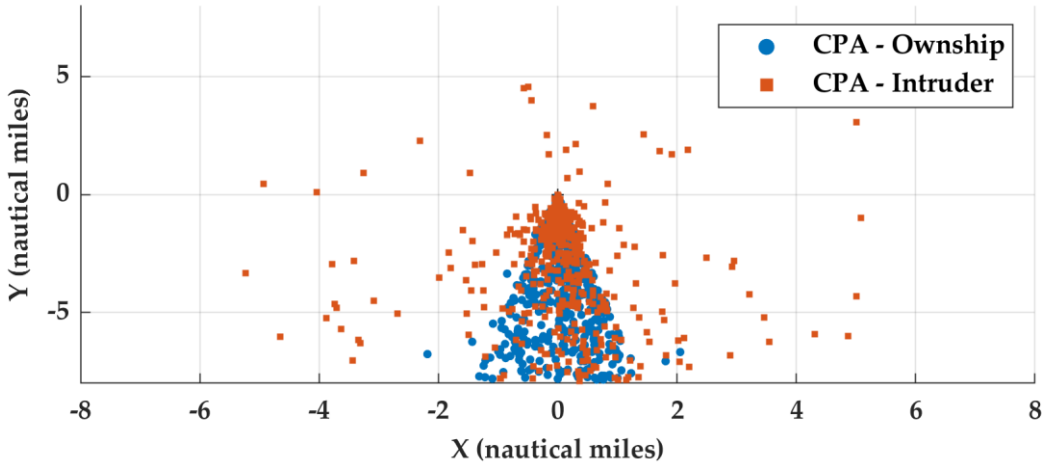

Figure 29. Sampled positions at CPA when ownship is taking off and intruder is landing.

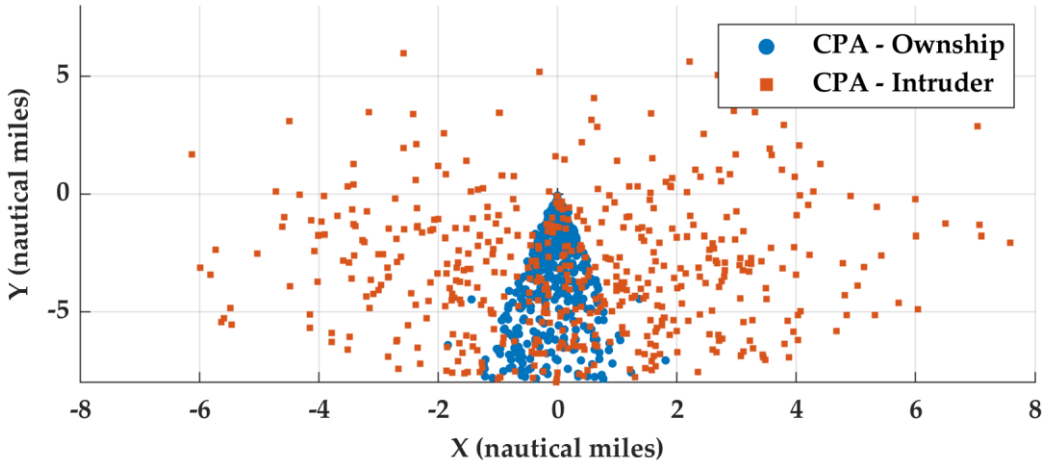

Figure 30. Sampled positions at CPA when ownship is taking off and intruder is transiting.

These figures illustrate two important elements of the model. First, the coordinate system is oriented such that ownship's runway is parallel to the y-axis, with positive down the runway from the threshold. This results in ownship predominately operating to the "south" of the runway and the cone shape of ownship's position is indicative of the 30 degree heading requirements for a straight landing or taking-off. Second, the intruder

Preprints (www.preprints.org) | NOT PEER-REVIEWED | Posted: 2 November 2021 doi:10.20944/preprints202111.0051.v1

position is dependent on its intent. Note in Figure 29 that a cluster of intruder positions are near (0,0) but this cluster is not evident in Figure 30. Also note that when transiting, the intruder at CPA is more dispersed. This was expected as transiting aircraft should not be operating predominantly along an approach or departure route. This is an outcome of the intent classification described in Section 2.3 and visually demonstrates how encounter geometry is dependent on aircraft intent.

2.6.2. Sampling the Trajectory Models to Propagate Tracks

Next, the ownship and intruder trajectories are successively sampled using the associated forwards and backwards trajectory generation models. Trajectories are propagated up to 120 one second timesteps before and after CPA, with initial positions provided by the geometry model sample. Propagation is halted if a trajectory is more than eight nautical miles from the runway mean position. Propagating the trajectories is achieved by successively sampling a trajectory model's variables from the top of the graph to the bottom, applying the learned conditional probabilities in conjunction with Bayes Rule. The trajectory models are sampled using a non-transitioning prior: absent observed information, dynamic variables remain constant. It is important to use these priors because the large space of discrete-valued variable combinations make it likely that there are gaps in the conditional probability tables. Sampling only gives discrete values for each of the model variables. Continuous values for the continuous variables must subsequently be sampled. In all cases, the model assumes this sampling will be from a uniform distribution within the relevant bin per the earlier tables.

Unlike previous encounter models, with which all transition events throughout an encounter can be sampled at once, the trajectory models can only be applied one time step at a time, with the new aircraft position being computed after each step. The new aircraft position is used to calculate the distance and bearing the track is away from the runway, with distance and bearing being model variables. This is required because distance from or bearing to the runway are not temporal variables in the Dynamic Bayesian network, as previously illustrated in Figure 14. The consequences of not dynamically modeling distance and bearing are illustrated by example encounters in Section 3.3 and further discussed in Section 4.

Also, unlike other MIT LL developed models, tracks do not need to fully overlap in time. It is possible for an encounter to start or end with only one aircraft in the vicinity of the runway. For example, an encounter could start at t = -120 seconds (prior to CPA) with the intruder initially positioned within 8 nautical miles of the runway. An ownship could be initialized at t = - 30 seconds near the runway at a low altitude to simulate the ownship beginning to take-off. In this example, CPA would occur at t = 0. At t = 30 seconds, the intruder could be more 8 nautical miles from the runway and no more track updates would be generated for it. From t = 31 and onward, only ownship would be simulated.

2.6.3. Rejection Sampling

Given an encounter of two aircraft tracks, we assess if its valid or should be rejected. If an encounter fails any of the described criteria, it is rejected and the encounter generation process is restarted with a new sample from the encounter geometry model. Criteria are organized into three categories: those based on training assumptions, assumptions unique to ownship, and dynamic constraints. The criteria based on training assumptions are designed such that the sampled synthetic encounters are subject to similar constraints and assumptions used to identify encounters for training, as described in Sections 2.2-2.4. These assumptions include:

- Encounter CPA must occur within 5 seconds of the sampled CPA from the geometry model;
- Tracks must overlap at least 30 seconds in time;
- If taking-off or landing, a track must have at least one track update within 2.5 nautical miles of the runway mean position;
- For track updates within 2.5 nautical miles of the runway mean position, at least one point must have an altitude of 750 feet or less;

Preprints (www.preprints.org) | NOT PEER-REVIEWED | Posted: 2 November 2021 doi:10.20944/preprints202111.0051.v1

- A track must have sufficient quantity of updates with a vertical rate magnitude of 300 feet per minute or greater. If landing, the rate must be negative and if taking off, the rate must be positive.
- A track ends if it is within 0.25 nautical miles of the runway.

Similar to when classifying track intent, ownship must satisfy a relative heading criterion, so it is representative of a straight landing or take-off. Given the coordinate system where the runway is parallel to the y-axis, a heading of 90 degrees would have the aircraft move positively ("north") along the y-axis and a heading of 270 degrees would have the aircraft move negatively along the y-axis. Thus, if an aircraft is initialized on the negative y-axis, a heading of 90 degrees would be towards of the runway and a heading of 270 degrees would be moving away from the runway. The Cartesian coordinate system is visualized with the example encounters in Figures 31-34. Accordingly, the ownship heading criteria is dependent upon intent:

- If landing, at least 95% of heading updates need to have a heading of 90 ± 30 degrees; and
- If taking off, at least 95% of heading updates need to have a heading of 270 ± 30 degrees.

The last set of criteria are enabled such that the ownship or intruder satisfied a set of dynamic limits on speed, acceleration, vertical rate, turn rate, and pitch angle. To support RTCA SC-228, we defined four sets of dynamic limits, summarized by Table 7. "Generic" limits are general limits applicable for a wide range of crewed aircraft. "RTCA228-A1" corresponds to the RTCA SC-228 assumptions for a HALE (High Altitude, Long Endurance) UAS, "RTCA228-A2" for an assumed MALE (Medium Altitude, Long Endurance) UAS and "RTCA228-A3" for an assumed LEPR (Low End Performance Representative). When rejection sampling for certain aircraft characteristics, that we are assume that the encounters for UAS will be the same as similarly operated crewed aircraft (e.g., same speeds, vertical rates, encounter geometry).

Of the dynamic limits, the acceleration limit was specifically based on the model structure and how trajectories are propagated. Since the trajectory models are sampled incrementally with intra-bin uniform sampling, it is possible to sample speed such that it transitions from 100 (bin 1) to 199 (bin 2) feet per second in one timestep. Since this would not be realistic, the maximum acceleration is based on the widest speed bin of 50 feet per second. This sampling criteria often results in tracks not changing speed during an encounter; this is illustrated in Section 3.2 and discussed as part of future work in Section 4.

Table 7. Dynamic limits when sampling encounters.

Variable (Units)	Generic	RTCA228-A1	RTCA228-A2	RTCA228-A3
Minimum speed (feet per second)	50	169	68	68
Maximum speed (feet per second)	506	491	338	186
Acceleration (feet per second^2)	50	50	50	50
Maximum vertical rate (feet per second)	100.00	41.67	25.00	8.34
Maximum turn rate (degrees per second)	12	1.5	3	7
Maximum pitch (degrees)	∞	15	15	15

3. Results

Preprints (www.preprints.org) | NOT PEER-REVIEWED | Posted: 2 November 2021 doi:10.20944/preprints202111.0051.v1

This section discusses the output of the model training with some statistics about the trained models, example encounters, and an overview of a dataset leveraged by RTCA SC-228 during FAA validation of the standard.

3.1. Encounter Statistics

Table 8 reports the number of encounters used to train the current encounter geometry model given airspace class and data source; Table 9 reports the distribution for the deprecated version 2 of the model. This distribution is synonymous with the encounters identified from the processing described in Section 2.5.

First, the quantity of Class C encounters significantly increased from version 2.0 to 3.0. Because version 2.0 assumed both aircraft were operating from the same runway, there were only 5 single-runway Class C airports considered to be in scope. We had relatively poor surveillance coverage for these airports and subsequently identified scant encounters. Expanding the model scope in version 3.0 to include different runway configurations and more airports resulted in a significant increase of identified encounters.

Second, expanding model scope in version 3.0 also resulted in a nearly 2000% increase of Class D encounters when using the OpenSky Network-based aerodromes dataset. This indicates that the majority of identified encounters were at airports with multiple runways. However, this does not imply that encounters are more or less frequent at single runway airports, because the ability to identify encounters was dependent on the surveillance coverage of the airport. It could be possible that both datasets had relatively poor surveillance coverage of single runway airports. Assessing surveillance coverage given airport design could be future work.

Third, the reduction of identified encounters in other airspace when using the terminal radar dataset was attributed to improvements in filtering traffic near other airports (Section 2.3.4). When classifying tracks for version 2.0, we did not consider the runway orientation and approach / departure corridors of nearby airports. As a result, tracks that were landing or taking off from nearby airports were misclassified as transiting intruders. As discussed in Section 2.3, the more advanced airport boundaries were generated for version 3.0 which reduced the misclassification of transiting tracks. This subsequently reduced the total quantity of identified encounters but the confidence that each encounter was within scope significantly improved.

Table 8. Model encounter based on data set and airspace class – Version 3.0.

Airspace Class	Terminal Radar	Aerodromes
B	2,396,048	1,038,390
C	103,566	81,253
D	85,514	45,066
Other (E/G)	1,209	432

Table 9. Model encounter based on data set and airspace class – Version 2.0 (deprecated).

Airspace Class	Terminal Radar	Aerodromes
B	0	0
C	10	5
D	65,859	2,150
Other (E/G)	6,784	169

Additionally, while the OpenSky Network-based training dataset had a greater spatial and temporal scope, it was limited to only identifying encounters between aircraft that both had ADS-B equipped. We hypothesize this bias is the key factor in the reduced encounter count compared to the terminal area radar dataset. The consequence of this bias was amplified because an ADS-B FAA mandate was not in effect until 2020, whereas the majority of the OpenSky Network data was from 2019 and before this mandate. To-

 doi:10.20944/preprints202111.0051.v1

day, ADS-B has also been mandated in most busy ATC controlled airspaces in the United States and there are various local, regional, and international roll-outs of ADS-B. As more aircraft equip ADS-B, we expect more encounters to be identified. Under investigation is how the training data, from any source, is dependent on ADS-B mandates, but this investigation is out of scope for this analysis.

Furthermore, when training version 2.0, we assessed that the transponder code filtering (Appendix B) did not have a significant impact on identifying encounters with the OpenSky Network based encounters. Without any Mode C filtering, 2,428 Class D encounters were identified, while with filtering 2,150 Class D encounters were identified. We did not repeat this analysis when training version 3.0.

3.2. Example Encounters

Figures 31–34 illustrate example encounters sampled from the model trained from terminal area radar tracks. Sampled encounters assume a generic aircraft type, and not necessarily reflective of the UAS dynamics from Table 7. Examples are intended to highlight the advantages and disadvantages of the model and rejection sampling approach to create encounters. In all the examples, the runway is oriented parallel to the y-axis. Tracks are illustrated as *peri-* or *intra-*. Track updates when only one aircraft is simulated at the timestep are noted as *peri-* while track updates when both aircraft are simulated are *intra-*.

3.2.1. Sampled Encounters

Figure 31 illustrates a sampled encounter where both aircraft are landing. While ownship must land straight, the intruder happens to also land straight but is not required to do so. The encounter starts at 120 seconds prior to CPA with only the ownship track simulated until 91 seconds prior to CPA when the intruder track is initialized about 8 nautical miles away from the runway. The ownship track ends shortly after CPA because it had a low enough altitude and close enough to the runway such that the tracks end. The intruder aircraft continues to be simulated until it also "lands" at 82 seconds after CPA. Since the models, as described in Section 2.5, have a minimum altitude of 200 feet, the lowest a track can be simulated to is also 200 feet. We also do not simulate tracks on the runway surface.

Preprints (www.preprints.org) | NOT PEER-REVIEWED | Posted: 2 November 2021 doi:10.20944/preprints202111.0051.v1

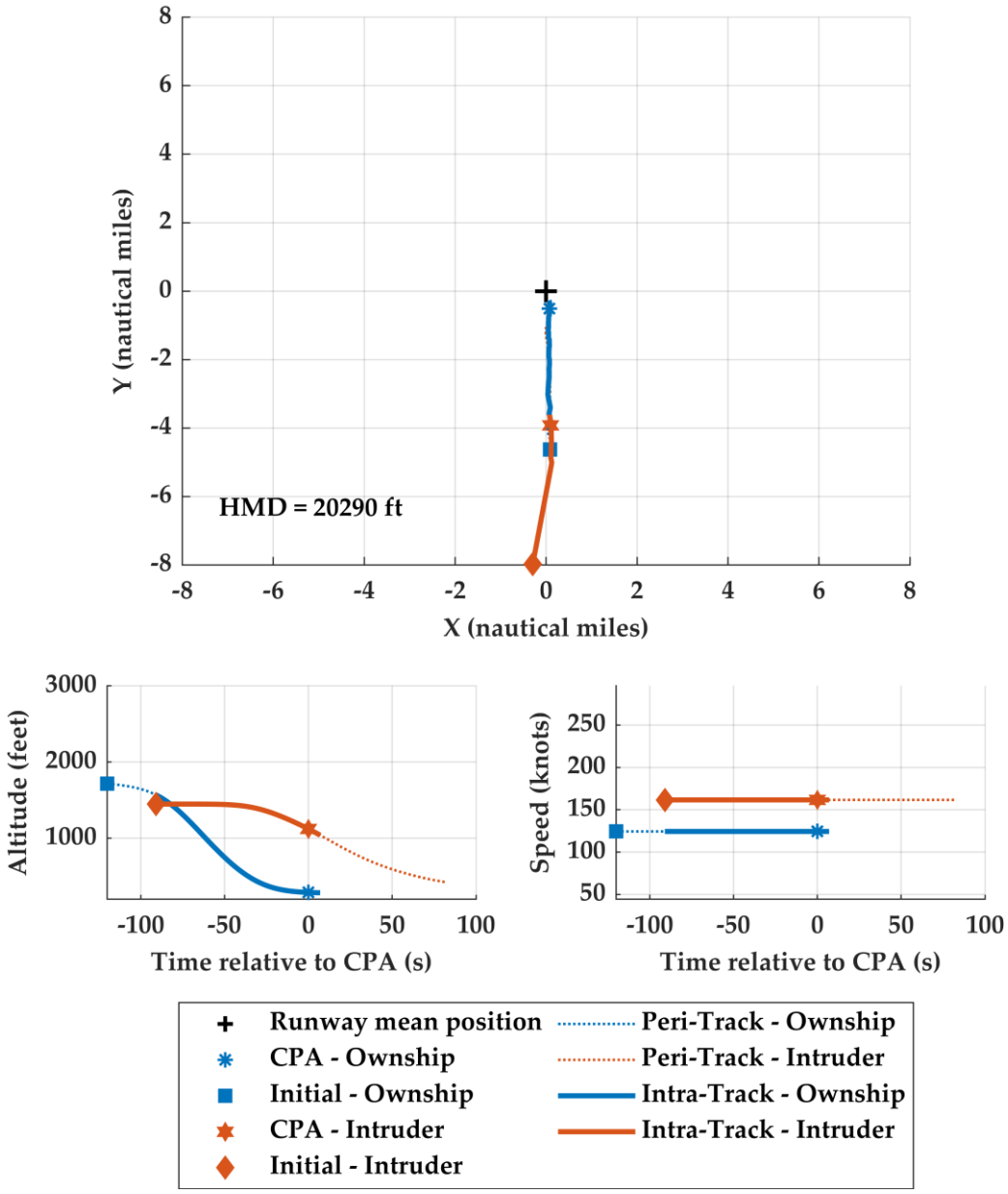

Figure 31 Sampled encounter where both aircraft are landing.

Figure 32 illustrates an encounter where ownship is taking off and the intruder is landing. Compared to Figure 31, Figure 32 demonstrates that a landing intruder does not have to be initialized along the negative y-axis, although it is common as in Figure 31. The intruder landing also has more heading changes and is not representative of a straight landing. Conversely, the ownship only has some minor heading changes.

Preprints (www.preprints.org) | NOT PEER-REVIEWED | Posted: 2 November 2021 doi:10.20944/preprints202111.0051.v1

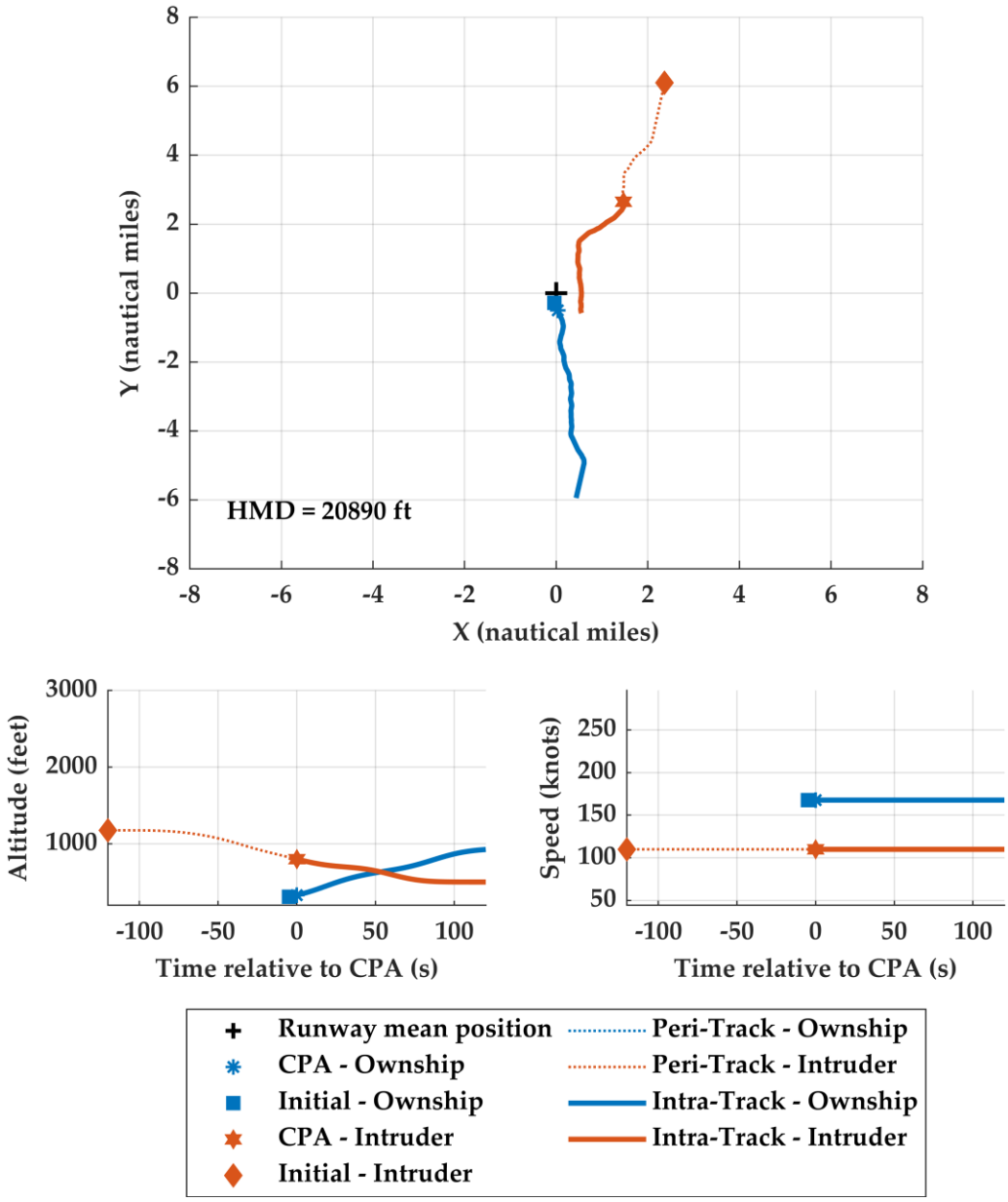

Figure 32. Sampled encounter where ownship is taking off and the intruder is landing.

Both of these examples also illustrate how model structure influences the simulated kinematics. Both vertical rate and speed are estimated from track updates with vertical rate derived from the difference between altitude reports and speed based on distance and bearing from the runway. Altitude is a temporal variable with (t) and (t+1) variables in the trajectory model but distance and bearing from the runway are not. Consequently, vertical rate is better modeled and more realistic. We rarely observe speed changes in sampled tracks. While this is undesired, we discuss in Section 4 why this is acceptable to support the RTCA SC-228 DAA validation but will be something explored further in the future.

3.2.2. Sampled Encounter with Transiting Intruders

Figure 33 illustrates an ownship taking off, like Figure 32, but has an intruder transiting through the airspace. Ownship exhibits similar features as in the previous examples with minimal heading changes, a reasonable vertical rate, and a constant speed. Since the coordinate system is centered on the assumed runway mean position, rather than an end of a runway, a track can be initialized anywhere near the origin, not necessarily on the y-axis. More importantly, this example illustrates how a transiting intruder behaves dif-

Preprints (www.preprints.org) | NOT PEER-REVIEWED | Posted: 2 November 2021 doi:10.20944/preprints202111.0051.v1

ferently than one taking off or landing. The intruder has a relatively constant altitude, more heading changes, and flies relatively farther away from the runway.

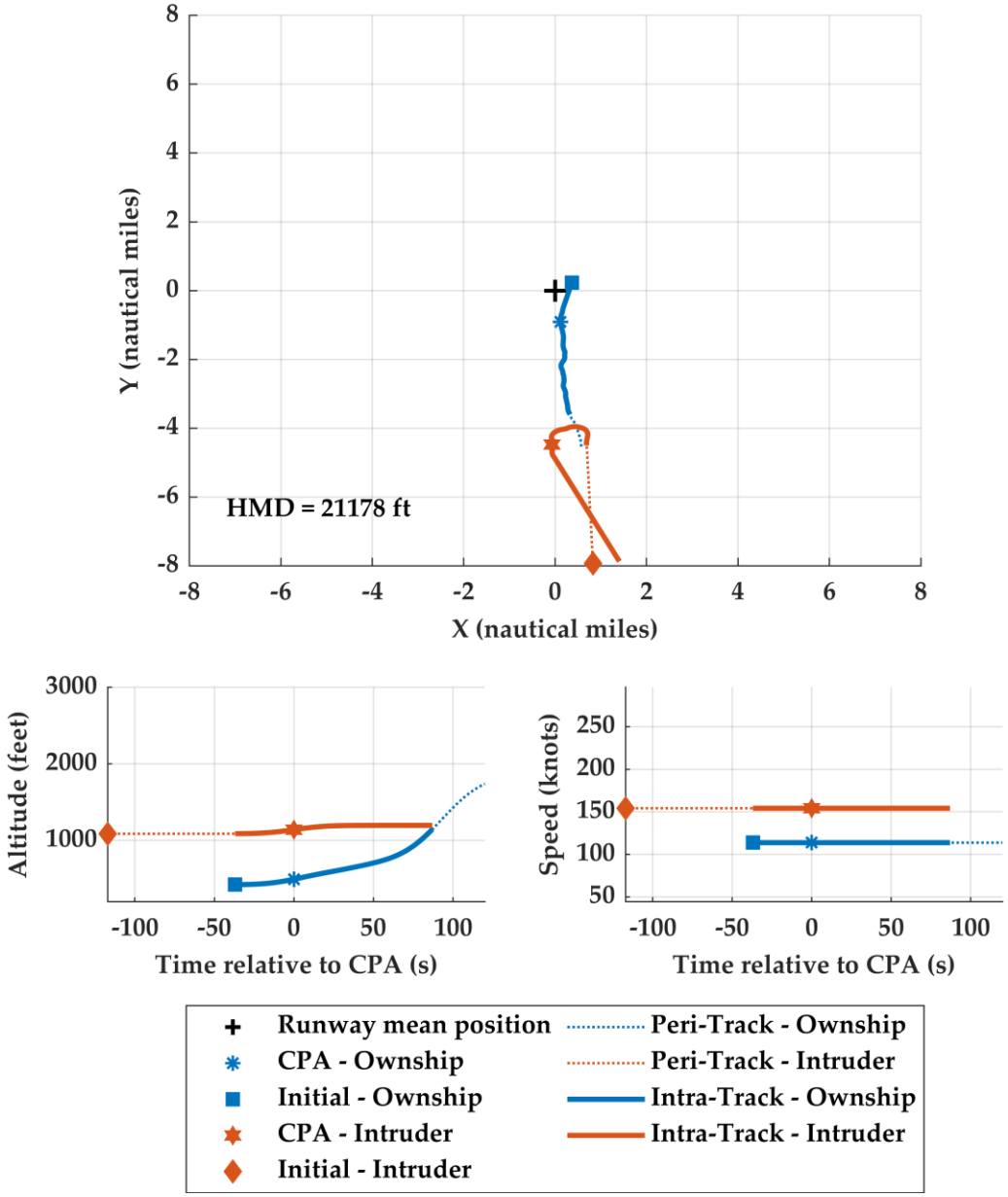

Figure 33. Sampled encounter where ownship is taking off and the intruder is transiting.

3.2.3. Sampled Encounter Idiosyncrasies

Like Figure 33, the last example encounter in Figure 34 illustrates an ownship taking off and an intruder transiting the airspace. The intruder maintains a relatively higher altitude and more lateral movement. Compared to the all the previous examples, transiting intruders have a wider range of potential behavior, as illustrated by the greater than 360 degree turn. Similar to the previous examples, ownship has minimal heading changes but exhibits an interesting altitude and vertical rate behavior. The ownship has an initial position within 2.5 nautical miles of the runway but at an altitude greater than 750 feet. The rejection sampling criteria, described in Section 2.6.3, is that at least one track update within 2.5 nautical miles of the runway must have an altitude of 750 feet or less and given that ownship is taking off, a sufficient number of track updates need to have a vertical rate of at least 300 feet per minute. Since the ownship immediately descends to an altitude below 750 feet, it satisfied the altitude criteria when near the runway. As the track climbs after CPA, it then also satisfied the vertical rate criteria.

Preprints (www.preprints.org) | NOT PEER-REVIEWED | Posted: 2 November 2021 doi:10.20944/preprints202111.0051.v1

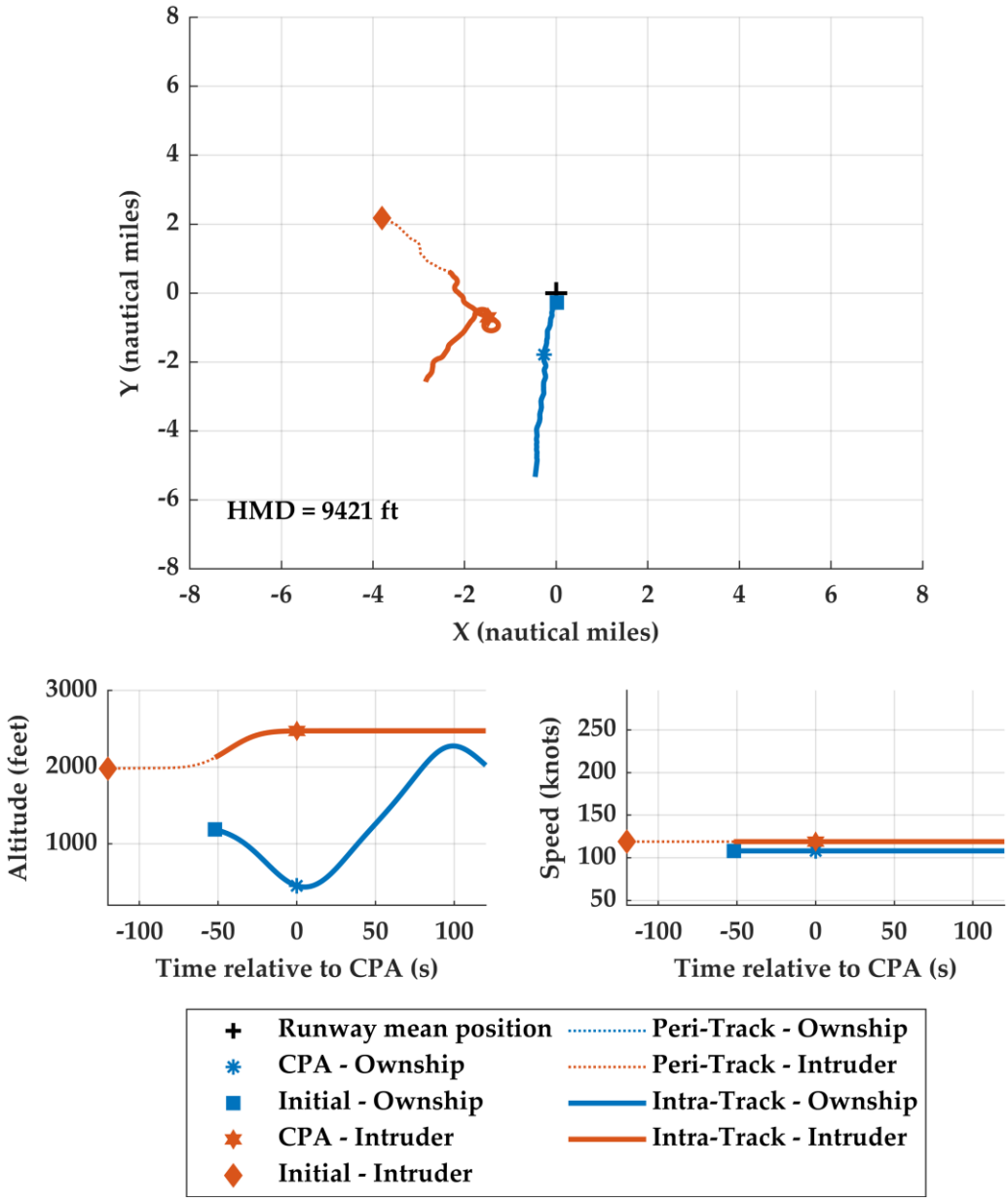

Figure 34. Sampled encounter where ownship is taking off and the intruder is transiting.

This example illustrates an advantage of using encounter models to support Monte Carlo simulations for safety evaluations. In practice, not all take-offs have a smooth vertical ascent and not all landings have smooth descents. This encounter also is not physically impossible and further validation is future work. While encounters like Figure 30 should be rare, it is reasonable to include them in safety assessments because they stress DAA systems in novel ways. Along with implications of a constant speed, the use of models and their idiosyncrasies are further discussed in Section 4.

3.3. Sampled Encounters to Support RTCA SC-228

Six million encounters were generated in total using both models trained on the terminal radar tracks and OpenSky Network. Three million encounters were sampled from each model, with one million encounters generated using the aircraft dynamic constraints for "RTCA228-A1," "RTCA228-A2," and "RTCA228-A3." For each of these million encounters, there was a uniform distribution over airspace class, ownship intent, and intruder intent.

 doi:10.20944/preprints202111.0051.v1

The encounters were simulated with the DEGAS simulation environment[38]. Encounters can be input to DEGAS as events or trajectories. Events specify the times at which a change in dynamics (e.g., turn rate, vertical rate, or acceleration) occurs, whereas trajectories specify the position (east, north, and altitude) of the aircraft at every time step. Events are simulated using a basic 6 degrees-of-freedom dynamics model, whereas trajectories, such as the encounters generated by sampling the terminal model, are followed directly (bypassing the dynamics model).

These encounters were used to assess key safety metrics in simulation for UAS terminal operations assuming a low latency networked terrestrial Command and Non-Payload Communications (CNPC) link that is aligned with the RTCA C2 MOPS and the use of a ground or airborne systems. The simulation assumed that the UAS was flying under IFR and receiving ATC separation services. Additionally, the simulation was designed to support a sensitivity analysis with the following objectives:

- Assessing the sensitivity of DAA system performance (safety and operational suitability) to C2 performance levels, and evaluation of the impact of relaxing C2 performance requirements;
- Identifying areas that should be targeted for future safety enhancements prioritized by maximum benefit; and
- Determining areas where small modeling variations may have a large impact on the safety metrics.

In response, we characterized the encounter sets based on aircraft kinematic states at CPA and the horizontal miss distance (HMD) and vertical miss distance (VMD) at CPA. Distributions were compared between the different models to characterize if the different training datasets led to different sampled encounters. Ultimately, training data sources have different biases and assumptions, so generating encounter sets using both modeled improved the robustness of the final simulation results for RTCA SC-228. Our discussion focuses on encounters with "RTCA228-A1" dynamic limits to narrow the discussion but we identified similar trends with the other encounter sets.

3.3.1. Kinematic Distributions at CPA

Figures 35 and 36 provide the distributions for distance from the runway, altitude, speed, and vertical rate for ownship and intruder at CPA. Ownship is using the "RTCA228-A1" dynamic limits while intruder is using the "generic" dynamic limits. Figure 35 was generated using the model trained using the terminal area radar tracks while Figure 36 used the OpenSky Network-based model. Histogram bins are based on the bins used by the encounter geometry model and may not be uniform.

Foremost, the altitude and vertical rate magnitude distributions were similar between the models. In general, the intruder was at lower altitude than the ownship at CPA, with both aircraft at 1500 feet or less. Extreme vertical rates were rarely observed at CPA, with most vertical rates of 10 feet per second (600 feet per minute) or less.

The distance at which CPA occurred from the runway slightly differed between the sampled encounter sets. While both encounter sets had about 75% of encounters within 4 nautical miles of the runway, the terminal area radar-based encounters had more encounters within one nautical mile of the runway, while the OpenSky Network-based encounters had a few more encounters at two to four nautical miles from the runway mean position. In support of the SRMD to assess DAA performance, these differences aren't particularly impactful because the DAA system is more influenced by the kinematics of which altitude and vertical rate had unimportant differences but there was a notable difference in the speed distributions.

For the terminal radar-based encounters, about 60% of encounters had ownship flying between 225 to 300 feet per second at CPA, while only 46% of OpenSky Network-based encounters had ownship at that speed at CPA. Also, only about 12% of intruders had a speed of 75 to 150 feet per second at CPA with the terminal radar-based encounters, compared to nearly 28% of the other encounter set. In general, the terminal radar-based encounters had a relatively faster "RTCA228-A1" UAS and relatively faster

Preprints (www.preprints.org) | NOT PEER-REVIEWED | Posted: 2 November 2021 doi:10.20944/preprints202111.0051.v1

"generic" intruder. Speeds greater than 300 feet per second (178 knots) at CPA were infrequently observed in about 7% of encounters in both sets.

Upon review of the encounters, we have a couple hypothesis to explain the differences in the speed distributions. Principally, aircraft type of fixed-wing or rotorcraft can be identified when training with the OpenSky Network-based model but not when using the terminal area radars. For the uncorrelated encounter models, we have observed models trained solely using observations of rotorcraft will have a speed distribution slower than models trained using solely fixed-wing aircraft[12]. An uncorrelated rotorcraft-based model also has a relatively slower speed distribution than a model trained using heterogenous mix of aircraft types. We hypothesized a similar trend is occurring with the terminal model, where the OpenSky Network-based model can leverage the aircraft type information and generate tracks that are more representative of relatively slower moving aircraft. An inspection of the model distributions given an aircraft type of rotorcraft support this hypothesis but additional validation is required. Additionally, due to ADS-B transponder equipage mandates, it is possible that more rotorcraft or general aviation fixed-wing single engine were equipped with transponders in 2018 than in 2015 when the terminal area radar dataset was curated. The models also inherently were trained based on different compositions of aircraft types, with the speed distributions reflecting these different compositions. This does not make either model incorrect but rather reflects a bias in the training data. We also enforced the desired uniform distribution over airspace, class, ownship intent, and intruder intent when rejection sampling.

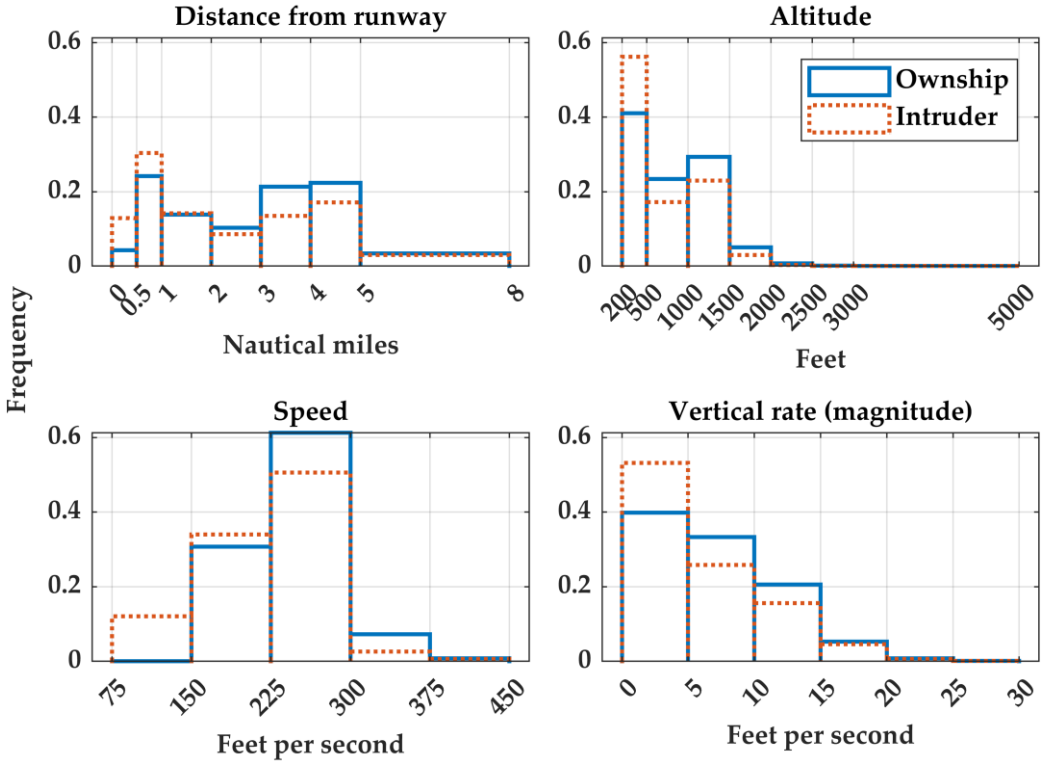

Figure 35. Distributions for kinematic variables at CPA for one million encounters with a "RTCA228-A1" ownship and "generic" intruder when using the terminal area radar trained model.

Preprints (www.preprints.org) | NOT PEER-REVIEWED | Posted: 2 November 2021 doi:10.20944/preprints202111.0051.v1

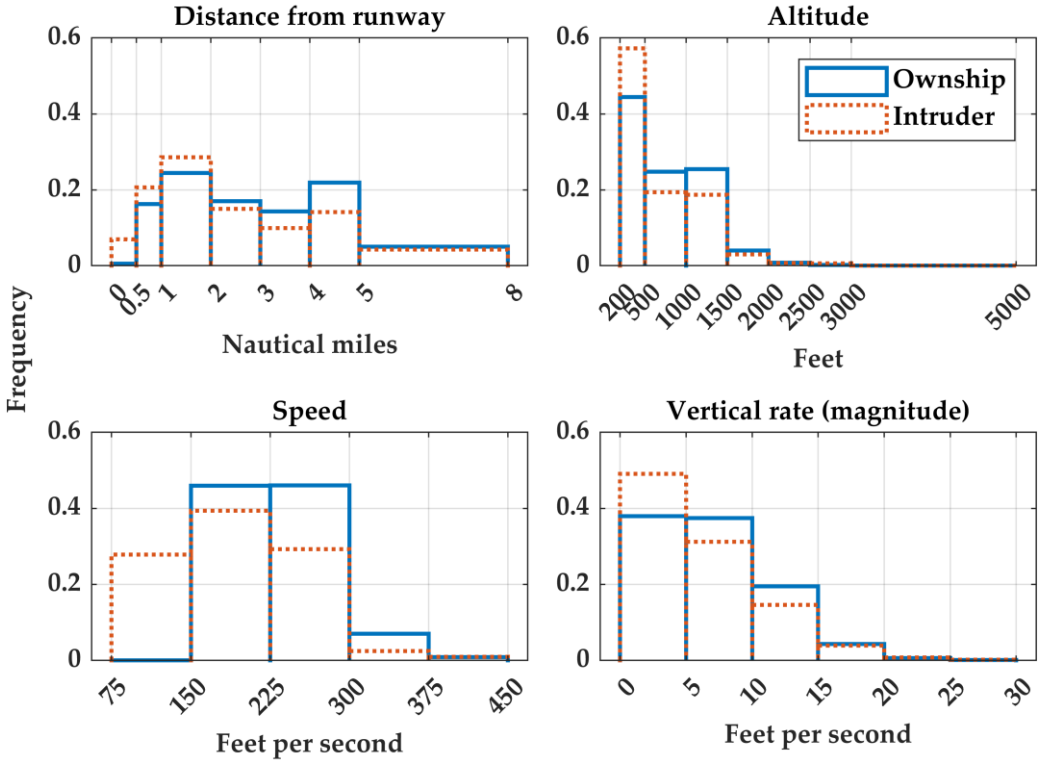

Figure 36. Distributions for kinematic variables at CPA for one million encounters with a "RTCA228-A1" ownship and "generic" intruder when using the OpenSky Network trained model.

3.3.2. Horizontal and Vertical Miss Distance Distributions

While independent aircraft speeds are important in characterizing an encounter, the closing speed between aircraft significantly influences the risk of a collision given an encounter and subsequently the HMD and VMD at CPA. The separation between aircraft is also based on other kinematic variables as well, such as relative heading between aircraft, aircraft turn rate, altitude, and vertical rate. Accordingly, Figures 37 and 38 plot the HMD and VMD distributions for the terminal area radar and OpenSky Network-based encounter sets with "RTCA228-A1" ownship and "generic" intruder. The distributions are illustrated as two dimensional CDF contour plots. Table 10 summarizes the CDF percentile given select HMD and VMD values. A positive VMD is indicative of the intruder above ownship and a negative VMD is when the ownship was above the intruder. For example, Figure 37 indicates that 25% of encounters sampled from the terminal area radar trained model, had an HMD of 7,000 feet or less and a VMD of 500 feet or less at CPA. Whereas 40% of encounters sampled from the OpenSky Network-based model satisfied these HMD and VMD thresholds.

These figures indicate that regardless of the model, majority of encounters had a CPA where the intruder was above the ownship. This can be attributed to transiting intruders which tend to have higher relative altitudes and the glide slope constraints on the ownship. The distributions also show that majority of encounters had a HMD and VMD greater than 2,200 and 450 feet respectively at CPA. This combination of HMD and VMD are notable as it a separation metric used by RTCA SC-228[39]–[41] and similar to separation criteria used by a different UAS DAA standard published by ASTM F38[16]. As the OpenSky Network-based model had 25% of encounters with a HMD and VMD of this or less, that encounter set was slightly more stressing to the DAA system and had encounters to estimate safety metrics based on that separation. As HMD and VMD at CPA increases, the distributions between the two encounter sets become more similar.

Preprints (www.preprints.org) | NOT PEER-REVIEWED | Posted: 2 November 2021 doi:10.20944/preprints202111.0051.v1

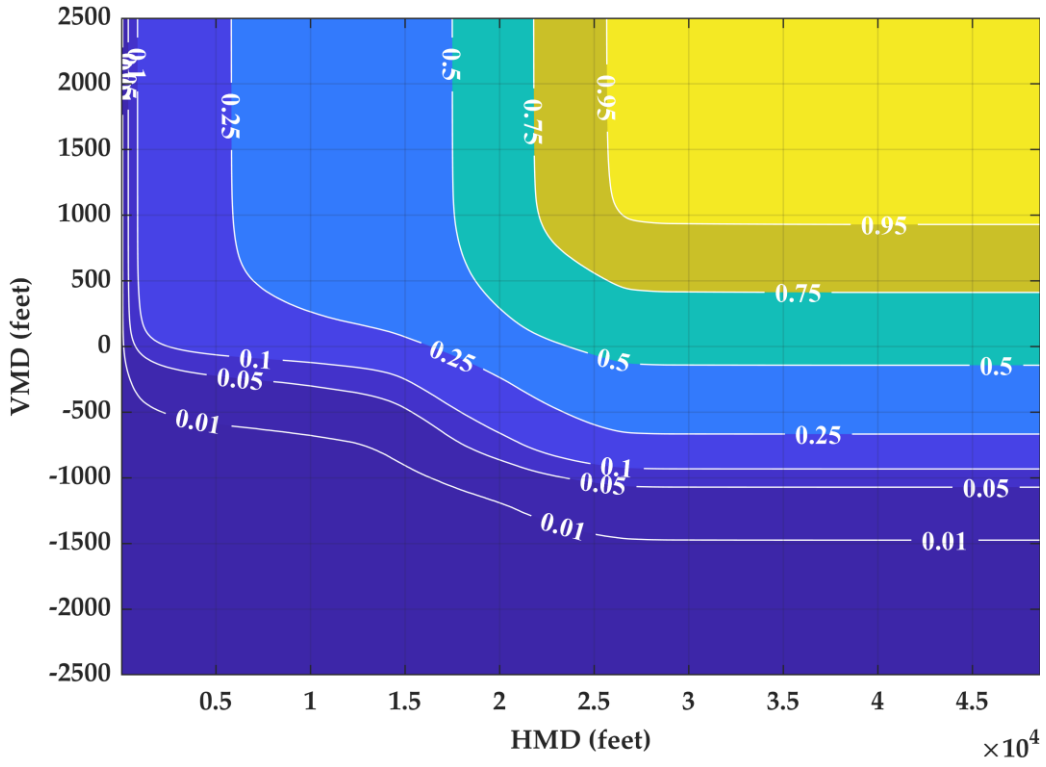

Figure 37. Distributions for HMD and VMD at CPA for one million encounters with a "RTCA228-A1" ownship and "generic" intruder when using the terminal area radar trained model.

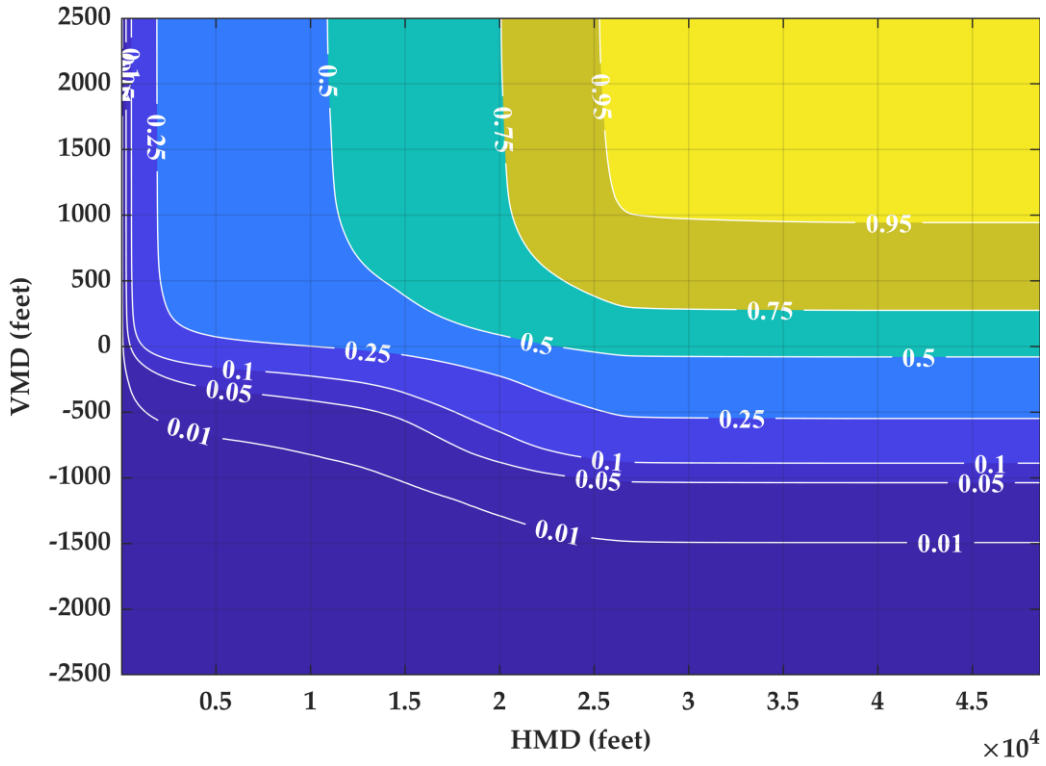

Figure 38. Distributions for HMD and VMD at CPA for one million encounters with a "RTCA228-A1" ownship and "generic" intruder when using OpenSky Network trained model.

Preprints (www.preprints.org) | NOT PEER-REVIEWED | Posted: 2 November 2021 doi:10.20944/preprints202111.0051.v1

Table 10. Select HMD and VMD fractiles for one million encounters with a "RTCA228-A1" ownship and "generic" intruder with models trained using different data.

HMD (feet)	VMD (feet)	Terminal Area Radars	OpenSky Network Aerodromes
2,200	450	0.17	0.25
2,500	0	0.10	0.15
2,500	250	0.16	0.25
7,000	500	0.25	0.40
16,400	0	0.25	0.34
23,600	0	0.50	0.51

4. Discussion on Future Work

Model development was still ongoing as of September 2021. We demonstrated the viability of a clustering approach to identify encounters based on assumptions of airport design, approach and departure routes, and aviation heuristics. When parallelizing across multiple processors on the LLSC, the approach identified a sufficient set of encounters for model training. While a trained model can generate reasonable encounters, the model structure introduces undesired dynamics and should be improved. Additionally, track classification for training and the model structure can be improved to better distinguish and model different track intents. Specifically, the current intruder intent of "transiting" can be too vague and likely insufficiently captures behavior tailored to terminal VFR or helicopter routes.

Regarding the use of the model for safety analyses, aircraft tracks were often initialized multiple nautical miles away from the runway and with faster airspeeds than associated with landings of rotorcraft, fixed-wing single-engine or smaller fixed-wing multi-engine aircraft. However, as discussed in Section 3.3.1, the modeled speeds at CPA were reasonable. There was no indication that aircraft were modeled with speeds slower than anticipated nor with unreasonably fast speeds at low altitudes. Collision risk increases with aircraft speed because closing speed also increases, which reduces the time required to loss of separation between aircraft. This was previously assessed for uncorrelated encounters with smaller UAS[42]. Given there exists some relationship between closing speed and risk, we assumed that the sampled encounters likely did not underestimate risk because the sampled encounters were presumed to not be slower than reality. Collision risk is not solely dependent on closing speed and there are other variables, many of which are encoded in the model itself. So, while modeled aircraft are not slowing down as they fly closer to the runway, additional validation is required to assess if the encounters slightly overestimated the risk due to the higher than expected speeds. Assuming fixed-wing aircraft have a minimum stall speed of 75-100 feet per second, we hypothesize that tracks could experience a speed change up to 85 feet per second over the course of an encounter in an improved model.

Using a classical Bayesian network to model where CPA occurred was shown to be practical and scalable, whereas many of the issues can be attributed to propagating tracks over the duration of the encounter. As such, model development will focus on improving how aircraft move through the airspace with respect the runway, rather than identifying where CPA or if an encounter was observed. Potential near-term future work includes aggregating the trajectory models into a one or two trajectory model with additional parent variables to denote if an aircraft is the ownship or intruder; or specifying additional, more specific intents such as "landing – straight," or "landing – any." Future work could also explore training a model using a hidden semi-Markov model, like Mahoubi and Kochenderfer[21], or with longer timesteps, such that, for example, track updates are sampled every ten instead of every one second. However, neither of these proposed developments would address issue of sampled speeds generally remaining constant.

It was insightful that vertical rate estimated from a temporal variable, altitude, was a better model than speed, which was not estimate from a temporal variable. While

Preprints (www.preprints.org) | NOT PEER-REVIEWED | Posted: 2 November 2021 doi:10.20944/preprints202111.0051.v1

we could prototype modifying the trajectory model such that distance and bearing from the runway are temporal variables, the current Dynamic Bayesian network structure is reliant upon discretized variables, which could produce similar intra-bin sampling issues.

One potential approach is to use aggregate or relative variables, instead of absolute variables in the model structure. Speed and vertical rate are currently absolute variables that models the absolute kinematics of the aircraft. An example aggregate variable would be the sum of aircraft speeds or the sum of vertical rates; while a potential relative variable would be the relative speed difference between the ownship and intruder. Using absolute, aggregate, and relative variables in combination could be memory efficient and better model the combinatorial state space of different aircraft kinematics. The use of aggregate states yielded promising results when previously exploring aircraft avoidance Markov Decision Processes (MDP)s[43].

Another approach similar to Mahboubi and Kochenderfer[21] could be prototyped where tracks can be classified by the probability of an aircraft transitioning from one navigation goal to the next. While Mahboubi and Kochenderfer used Turning Points as a navigation goal, goals could also be formulated origin and destination (O-D) pairs. O-D pairs have been used to model potential air taxi traffic between locations, with O-D pairs enabling models to assess various operational constraints between different structured routes[44]. Mahboubi and Kochenderfer modeled aircraft navigation between stochastic O-D pairs, the parameters and nodes of the models were hand engineered based on a nominal traffic pattern, while demonstrating they could be learned from observations.

We hypothesize that instead of a network based on specific phases of a terminal operation, such as states associated with a 45 degree entry into a downwind, turn onto base, and a turn into final before landing. Using the existing or modified model structure, Dynamic Bayesian Network(s) could be trained for each state. For example, consider a terminal environment with a single runway and VFR route. The VFR route could be composed of multiple waypoints but the proposed model would represent the entire VFR route as a single state. Similar to the cluster approach described in Section 2.3, we could identify tracks with a VFR route state. Subsequently, states associated with landing or taking-off from the ends of the runway would have their own states. Given this state classification, we could train models tailored to the states. Then similar to the encounter identification approach from Section 2.4, we could identify encounters given navigational state and relative position. This should enable the model to better distinguish between an intruder flying along a VFR route with specific operating rules and assumptions and an intruder transiting through the airspace at relatively higher altitudes. Each state could have a Dynamic Bayesian network to model how aircraft operate within a state (i.e., flying along the VFR route) with a separate Bayesian network to model the transition between states. This hierarchical model would then enable modeling of both aircraft kinematics and the relative interactions between navigational states. Notwithstanding, future work will focus on improving modeled speed and various intents.

Other avenues for future work include rotorcraft track identification with techniques that do not leverage the aircraft registry, such as using an autoencoder[45] or kinematic features[46]; considerations for nonconventional aircraft, such as gliders or balloons; or incorporate traffic flow management concepts[47] into our model.

5. Conclusions

We overview the development of a statistical model of how crewed aircraft behave when operating in terminal airspace and a rejection sampling approach to create encounters representative of those with uncrewed aircraft. Using the trained models, we can develop and evaluate systems that mitigate airborne collision risk. Specifically, the models directly support activities of the RTCA SC-228 standards development committee.

6. Patents

No patents resulted from the reported work.

Supplementary Materials:

Andrew Weinert, "Validating Encounter Model Assumptions and Representativeness for the Class B Environment," Oct. 13, 2021. doi: 10.5281/zenodo.5539498

Andrew Weinert, Marc Brittain, Ngaire Underhill and Christine Serres, "Benchmarking the Processing of Aircraft Tracks with Triples Mode and Self-Scheduling", Sep. 01, 2021. doi: 10.5281/zenodo.5338796

Andrew Weinert, "Correlated Bayesian Model of Aircraft Encounters in the Terminal Area Given a Straight Takeoff or Landing", Jul. 06, 2021. doi: 10.5281/zenodo.5076477

Author Contributions: Conceptualization, A.W, N.U, C.S, and R.G; Data curation, A.W, N.U, C.S, and R.G; Formal analysis, A.W, N.U, C.S, and R.G; Funding acquisition, A.W and R.G; Investigation, A.W, N.U, C.S, and R.G; Methodology, A.W, N.U, C.S, and R.G; Project administration, A.W and R.G; Software, A.W, N.U, C.S, and R.G; Supervision, A.W and R.G; Validation, A.W, N.U, and C.S; Visualization, A.W; Writing – original draft, A.W, N.U, C.S, and R.G; Writing – review & editing, A.W.

Funding: DISTRIBUTION STATEMENT A. Approved for public release. Distribution is unlimited.. This material is based upon work supported by the Federal Aviation Administration under Air Force Contract No. FA8702-15-D-0001. Any opinions, findings, conclusions or recommendations expressed in this material are those of the author(s) and do not necessarily reflect the views of the Federal Aviation Administration. Delivered to the U.S. Government with Unlimited Rights, as defined in DFARS Part 252.227-7013 or 7014 (Feb 2014). Notwithstanding any copyright notice, U.S. Government rights in this work are defined by DFARS 252.227-7013 or DFARS 252.227-7014 as detailed above. Use of this work other than as specifically authorized by the U.S. Government may violate any copyrights that exist in this work.

Data Availability Statement: Associated datasets can be found at https://zenodo.org/communities/airspace-encounter-models/ or https://www.ll.mit.edu/r-d/datasets; and associated software can be found at https://github.com/airspace-Encounter-Models/em-model-manned-bayes.

Acknowledgments: The authors greatly appreciate the support provided by Sabrina Saunders-Hodge and Deepak Chauhan from the Federal Aviation Administration. The authors wish to acknowledge the support of their colleagues, Dr. Rodney Cole and Matthew Edwards. The authors also acknowledge the MIT Lincoln Laboratory Supercomputing Center for providing high performance computing resources that have contributed to the research results reported within this paper.

Conflicts of Interest: The authors declare no conflict of interest. The funders had a role in the decision to publish the results.

Appendix A

This appendix lists the FAA airports that were in scope for the version 2.0 of the terminal encounter model. The quantity of observations near these airports varied, due to surveillance coverage and characteristics of the sources of aircraft tracks. Some locations had little to no observations. Specifically, FAA Class C airports that were in scope included:

- KAVL
- KBGR
- KGSP
- KMYR
- KRSW

FAA Class D airports that were in scope included:

- KADS

Preprints (www.preprints.org) | NOT PEER-REVIEWED | Posted: 2 November 2021 doi:10.20944/preprints202111.0051.v1

- KARA
- KASE
- KASH
- KBCT
- KBLI
- KBVI
- KCGF
- KCHO
- KCKB
- KCRE
- KCRQ
- KCWF
- KEMT
- KEYW
- KFLG
- KFUL
- KFYV
- KGCN
- KGKY
- KGTR
- KGUS
- KGVT
- KGYR
- KHHR
- KHSA
- KHTS
- KIFP
- KJAC
- KLAW
- KLBE
- KLWB
- KLZU
- KMDT
- KMER
- KMFR
- KMGW
- KMRB
- KMTN
- KNQA
- KOJC
- KOXC
- KOXR
- KPSM
- KRME
- KRNT
- KROG
- KRYY
- KSAW
- KSBD
- KWHP
- KPAO
- KGEU
- KSDL
- KSGR
- KSKF

Preprints (www.preprints.org) | NOT PEER-REVIEWED | Posted: 2 November 2021 doi:10.20944/preprints202111.0051.v1

- KSMO
- KSQL
- KSUN
- KTBN
- KTIW
- KTTD
- KTUP
- KVOK
- KWJF
- KWRB
- KXMR
- KHQZ
- KTKI

There were 873 FAA Class E and G airports considered in scope for this analysis. Please contact the authors for a complete list of these airports.

Appendix B

When identifying encounters as part of model training, all observations of aircraft transmitting any of the special transponder codes in the following table were rejected.

Table 6. Special use transponder codes not used for model training.

Code	Purpose
1206	VFR law enforcement, first responder by L.A., may not be in contact with ATC
1255	Firefighting aircraft
1273-1275	Calibration and performance monitoring equipment
1276	Air defense identification zone penetration (when unable to contact ATC or aeronautical facility)
4401-4433, 4466-4477	Special aircraft - sensitive unclassified
4434-4437	Weather reconnaissance
4447-4452	Special flight support codes
5000-5057, 5063-5077, 5400, 6100, 6400, 7501-7577	DOD reserved codes only to be assigned by NORAD
5100-5300	More DOD aircraft
7400	Reserved for uncrewed aircraft with a lost link
7500	Hijack
7600	Radio failure
7601-7607, 7701-7707	Allocated by the FAA for special use by law enforcement agencies
7700	Emergency
7777	DOD interceptor aircraft on active air defense missions -operating without ATC clearance

Appendix C

This appendix overviews the initial approach of version 1.0 to identify if a runway was for taking off or landing. This approach was found to be sensitive to false positive identifications (e.g., wrong runway identified or assessed as landing but actually transiting). The criteria were tuned to minimize such false positives at the expense of excluding some otherwise relevant trajectories (i.e., false negatives). In response, the approach described in Section 2 was developed to reduce misidentifications, enhance the robust-

 doi:10.20944/preprints202111.0051.v1

ness and improve scalability. For reference, we overview the original deprecated approach in this appendix.

Each trajectory was separately assessed for landing and for takeoff, so it can be tagged as one or the other, both, or neither. The procedure for both takeoff runway and landing runway identification entails transforming the latitude/longitude trajectory into a Cartesian coordinate frame centered on each candidate runway.

For takeoffs, the assessment is limited to the first 30 seconds of trajectory data. That trajectory segment is assessed against the following criteria to determine if the runway remains a candidate:

- Trajectory segment include altitude below 1500 feet (relative to runway elevation);
- The segment is generally increasing in altitude;
- The ground track is aligned within 45° of the runway; and
- The segment includes positive points on the along-runway axis that are within 4000 feet of the runway laterally.

If no runways satisfy these criteria, the trajectory is not a takeoff. (Conceivably some takeoff trajectories will be missed if they begin at the defined edge of the terminal area, land, and immediately take off again.) If a single runway satisfies the criteria, the trajectory is marked as a takeoff from that runway. If multiple runways satisfy the criteria, the trajectory is marked as a takeoff from the runway with threshold closest in ground range to the initial point on the trajectory.

For landings, a similar procedure is followed. The assessment uses the final 30 seconds trajectory data, which must satisfy the following criteria for a runway to remain a candidate:

- Includes altitudes below 1500 feet (relative to runway elevation);
- Ground track is aligned within 35° of runway; and
- Includes negative points on the along-runway ways that are within 4000 feet of the runway laterally.

As for takeoffs, if multiple runways satisfy the criteria, the runway with threshold closest in ground range to the final point of the trajectory segment is identified as the landing runway. Note that this procedure likewise will miss the scenario outlined above where the landing and takeoff occur in the middle of the trajectory. Both assessments neglect any events in the middle of the trajectory and do not assess, for example, intermediate landings and takeoffs in trajectories with multiple go-arounds.

Any landing trajectories are also assessed for using a straight-in approach, which would make the trajectory applicable as a surrogate UAS trajectory. Straight-in approaches require that the aircraft make no turns after passing the Final Approach Fix, which is different for every airfield but typically four to five miles from the runway. This criterion is simplified to whether the trajectory (not just the 60-second segment) passes within one nautical mile laterally when it is at four nautical miles along the negative along-runway axis.

Finally, encounters are identified amongst the landing and taking off trajectories. To be identified as such, one track must be a straight-in landing (the surrogate uncrewed aircraft) and the second track must be a landing (either straight-in or otherwise) and/or takeoff.

Appendix D

For the encounter set generated to support RTCA SC-228, trajectory data is provided in two forms: a single binary file containing position points for all encounters (along-runway position (ft), cross-runway position (ft), and altitude (ft)), and full state data (position/velocity/attitude) in individual text files for each aircraft and each encounter. The following variables are included in the full state data:

- Time (in seconds)
- Speed (in feet per second)
- Track Angle (in radians)

 doi:10.20944/preprints202111.0051.v1

- Bank Angle (in radians)
- Pitch Angle (in radians)
- Acceleration (in feel per second squared)
- Along-Runway Position (in feet)
- Cross-Runway Position (in feet)
- Altitude (relative to runway elevation, in feet)
- Along-Runway Velocity (in feet per second)
- Cross-Runway Velocity (in feet per second)
- Vertical Speed (in feet per second)
- Heading Rate (in radians per second)
- Latitude (in degrees)
- Longitude (in degrees)

The latitude and longitude values assume a runway at a fixed geodetic location oriented due north. An additional metadata file indicates the sampled encounter conditions as well as CPA information for each encounter. Metadata is formatted to align with the DAIDALUS algorithm [7]. The following variables are included in the metadata:

- Encounter ID
- Airspace class (1 – Class D, 2 – Class E, 3 – Class G)
- Ownship intent (-1 – landing, 1– takeoff)
- Intruder intent (-1 – landing, 0 – transit, 1– takeoff)
- Intruder type (1 – fixed wing)
- Intruder runway (1 – same)
- Ownship distance from runway at CPA (in nautical miles)
- Ownship bearing relative to runway at CPA (in degrees)
- Ownship altitude at CPA (in feet relative to airport elevation)
- Ownship speed at CPA (in feet per second)
- Ownship track relative to runway at CPA (in degrees)
- Ownship vertical rate at CPA (in feet per minute)
- Intruder distance from runway at CPA (in nautical miles)
- Intruder bearing relative to runway at CPA (in degrees)
- Intruder altitude at CPA (in feet relative to airport elevation)
- Intruder speed at CPA (in feet per second)
- Intruder track relative to runway at CPA (in degrees)
- Intruder vertical rate at CPA (in feet per minute)
- Ownship initial altitude (in feet relative to airport elevation)
- Ownship initial speed (in feet per second)
- Ownship initial vertical rate (in feet per minute)
- Intruder initial altitude (in feet relative to airport elevation)
- Intruder initial speed (in feet per second)
- Intruder initial vertical rate (in feet per minute)
- Time of CPA (in seconds)
- Horizontal miss distance (in feet)
- Vertical miss distance (in feet)
- Whether a Near Mid-Air Collision (500 ft horizontally, 100 ft vertically) occurred (1 = yes, 0 = no)

References

[1] International Civil Aviation Organization, "Global Air Traffic Management Operational Concept," Doc 9854 AN/458, 2005.

[2] L. P. Espindle, J. D. Griffith, and J. K. Kuchar, "Safety Analysis of Upgrading to TCAS Version 7.1 Using the 2008 U.S. Correlated Encounter Model," Massachusetts Institute of Technology, Lincoln Laboratory, Lexington, MA, Project Report ATC-349, 2009.

[3] "Terms of Reference RTCA Special Committee 228: Minimum Performance Standards for Unmanned Aircraft Systems (Rev 10)," RTCA, RTCA Paper 163-20/PMC-2034, Jun. 2020.

[4] S. P. Cook, D. Brooks, R. Cole, D. Hackenberg, and V. Raska, "Defining Well Clear for Unmanned Aircraft Systems," Jan. 2015. doi: 10.2514/6.2015-0481.

[5] Ghatas, Rania W and Jack, Devin P and Tsakpinis, Dimitrios and Vincent, Michael J and Sturdy, James L and Munoz, Cesar A and Hoffler, Keith D and Dutle, Aaron M and Myer, Robert R and Dehaven, Anna M and Lewis, Elliot T and Aruther, Keith E, "Unmanned Aircraft Systems Minimum Operations Performance Standards End-to-End Verification and Validation (E2-V2) Simulation," NASA Langley Research Center, Hampton, VA, Technical Report NASA/TM-2017-219598, Apr. 2017. [Online]. Available: https://ntrs.nasa.gov/search.jsp?R=20170004506

[6] "DO-365 - Minimum Operational Performance Standards (MOPS) for Detect and Avoid (DAA) Systems," RTCA, Minimum Operational Performance Standards DO-365A, May 2017.

[7] C. Muñoz *et al.*, "DAIDALUS: Detect and Avoid Alerting Logic for Unmanned Systems," in *2015 IEEE/AIAA 34th Digital Avionics Systems Conference (DASC)*, Sep. 2015, pp. 5A1-1-5A1-12. doi: 10.1109/DASC.2015.7311421.

[8] M. P. Owen, A. Panken, R. Moss, L. Alvarez, and C. Leeper, "ACAS Xu: Integrated Collision Avoidance and Detect and Avoid Capability for UAS," in *2019 IEEE/AIAA 38th Digital Avionics Systems Conference (DASC)*, Sep. 2019, pp. 1–10. doi: 10.1109/DASC43569.2019.9081758.

[9] M. W. Edwards, M. J. Kochendedrfer, J. K. Kuchar, and L. P. Espindle, "Encounter Models for Unconventional Aircraft, Version 1.0," Massachusetts Institute of Technology, Lincoln Laboratory, Lexington, MA, Project Report ATC-348, 2009.

[10] M. J. Kochenderfer, M. W. M. Edwards, L. P. Espindle, J. K. Kuchar, and J. D. Griffith, "Airspace Encounter Models for Estimating Collision Risk," *Journal of Guidance, Control, and Dynamics*, vol. 33, no. 2, pp. 487–499, Apr. 2010, doi: 10.2514/1.44867.

[11] A. J. Weinert, E. P. Harkleroad, J. D. Griffith, M. W. Edwards, and M. J. Kochenderfer, "Uncorrelated Encounter Model of the National Airspace System Version 2.0," Massachusetts Institute of Technology, Lincoln Laboratory, Lexington, MA, Project Report ATC-404, Aug. 2013.

[12] N. Underhill and A. Weinert, "Applicability and Surrogacy of Uncorrelated Airspace Encounter Models at Low Altitudes," *Journal of Air Transportation*, pp. 1–5, May 2021, doi: 10.2514/1.D0254.

[13] M. J. Kochenderfer, L. P. Espindle, J. K. Kuchar, and J. D. Griffith, "Correlated Encounter Model for Cooperative Aircraft in the National Airspace System," Massachusetts Institute of Technology, Lincoln Laboratory, Lexington, MA, Project Report ATC-344, 2008.

[14] N. Underhill, E. Harkleroad, R. Guendel, A. Weinert, D. Maki, and M. Edwards, "Correlated Encounter Model for Cooperative Aircraft in the National Airspace System; Version 2.0," Massachusetts Institute Technology Lincoln Laboratory Lexington United States, Lexington, MA, Project Report ATC-440, May 2018. Accessed: Jan. 16, 2019. [Online]. Available: https://apps.dtic.mil/docs/citations/AD1051496

[15] L. E. Alvarez, I. Jessen, M. P. Owen, J. Silbermann, and P. Wood, "ACAS sXu: Robust Decentralized Detect and Avoid for Small Unmanned Aircraft Systems," in *2019 IEEE/AIAA 38th Digital Avionics Systems Conference (DASC)*, Sep. 2019, pp. 1–9. doi: 10.1109/DASC43569.2019.9081631.

[16] ASTM International, "F3442/F3442M-20 Standard Specification for Detect and Avoid System Performance Requirements," ASTM International, West Conshohocken, PA, 2020. [Online]. Available: https://doi.org/10.1520/F3442_F3442M-20

[17] A. Weinert, N. Underhill, and A. Wicks, "Developing a Low Altitude Manned Encounter Model Using ADS-B Observations," in *2019 IEEE Aerospace Conference*, Big Sky, MT, Mar. 2019, pp. 1–8. doi: 10.1109/AERO.2019.8741848.

[18] A. Weinert *et al.*, *Airspace-Encounter-Models/em-model-manned-bayes: July 2021 - Terminal Model and Improved Performance*. Zenodo, 2021. doi: 10.5281/zenodo.5113936.

[19] A. Weinert *et al.*, *Airspace-Encounter-Models/em-model-manned-bayes: October 2021*. Zenodo, 2021. doi: 10.5281/zenodo.5544340.

[20] M. Gariel, A. N. Srivastava, and E. Feron, "Trajectory Clustering and an Application to Airspace Monitoring," *IEEE Transactions on Intelligent Transportation Systems*, vol. 12, no. 4, pp. 1511–1524, Dec. 2011, doi: 10.1109/TITS.2011.2160628.

[21] Z. Mahboubi and M. J. Kochenderfer, "Learning Traffic Patterns at Small Airports From Flight Tracks," *IEEE Transactions on Intelligent Transportation Systems*, vol. 18, no. 4, pp. 917–926, Apr. 2017, doi: 10.1109/TITS.2016.2598064.

[22] S. T. Barratt, M. J. Kochenderfer, and S. P. Boyd, "Learning Probabilistic Trajectory Models of Aircraft in Terminal Airspace From Position Data," *IEEE Transactions on Intelligent Transportation Systems*, pp. 1–10, 2018, doi: 10.1109/TITS.2018.2877572.

[23] L. Li, M. Gariel, R. J. Hansman, and R. Palacios, "Anomaly detection in onboard-recorded flight data using cluster analysis," in *2011 IEEE/AIAA 30th Digital Avionics Systems Conference*, Oct. 2011, pp. 4A4-1-4A4-11. doi: 10.1109/DASC.2011.6096068.

[24] L. Li, R. J. Hansman, R. Palacios, and R. Welsch, "Anomaly detection via a Gaussian Mixture Model for flight operation and safety monitoring," *Transportation Research Part C: Emerging Technologies*, vol. 64, pp. 45–57, Mar. 2016, doi: 10.1016/j.trc.2016.01.007.

[25] J. Krozel, "Intelligent Tracking of Aircraft in the National Airspace System," in *AIAA Guidance, Navigation, and Control Conference and Exhibit*, American Institute of Aeronautics and Astronautics, 2002. doi: 10.2514/6.2002-4995.

[26] H. Georgiou, N. Pelekis, S. Sideridis, D. Scarlatti, and Y. Theodoridis, "Semantic-aware aircraft trajectory prediction using flight plans," *Int J Data Sci Anal*, vol. 9, no. 2, pp. 215–228, Mar. 2020, doi: 10.1007/s41060-019-00182-4.

[27] A. M. Churchill and M. Bloem, "Clustering Aircraft Trajectories on the Airport Surface," Chicago,IL, USA, 2019.

[28] M. Schäfer, M. Strohmeier, V. Lenders, I. Martinovic, and M. Wilhelm, "Bringing up OpenSky: A large-scale ADS-B sensor network for research," in *IPSN-14 Proceedings of the 13th International Symposium on Information Processing in Sensor Networks*, Apr. 2014, pp. 83–94. doi: 10.1109/IPSN.2014.6846743.

[29] A. Weinert, M. Brittain, C. Serres, and N. Underhill, *mit-ll/em-download-opensky: Initial release*. Zenodo, 2020. doi: 10.5281/zenodo.4329768.

[30] K. Dube, G. Nhamo, and D. Chikodzi, "COVID-19 pandemic and prospects for recovery of the global aviation industry," *Journal of Air Transport Management*, vol. 92, p. 102022, May 2021, doi: 10.1016/j.jairtraman.2021.102022.

[31] A. Weinert, N. Underhill, B. Gill, and A. Wicks, "Processing of Crowdsourced Observations of Aircraft in a High Performance Computing Environment," in *2020 IEEE High Performance Extreme Computing Conference (HPEC)*, Sep. 2020, pp. 1–6. doi: 10.1109/HPEC43674.2020.9286229.

[32] A. Weinert, M. Brittain, C. Serres, and R. Guendel, "Benchmarking the Processing of Aircraft Tracks with Triples Mode and Self-Scheduling," in *2021 IEEE High Performance Extreme Computing Conference (HPEC)*, Jun. 2021, pp. 1–8.

[33] W. A. Olson and J. E. Olszta, "TCAS Operational Performance Assessment in the U.S. National Airspace," in *29th Digital Avionics Systems Conference*, Oct. 2010, p. 4.A.2-1-4.A.2-11. doi: 10.1109/DASC.2010.5655351.

[34] A. Weinert, M. Brittain, and R. Guendel, "Frequency of ADS-B Equipped Manned Aircraft Observed by the OpenSky Network," *Proceedings*, vol. 59, no. 1, Art. no. 1, 2020, doi: 10.3390/proceedings2020059015.

[35] "National Plan of Integrated Airport Systems (NPIAS), 2015-2019," Federal Aviation Adminstration, Report to Congress, Sep. 2014.

[36] M. J. Kochendedrfer, L. P. Espindle, J. K. Kuchar, and J. D. Griffith, "A Comprehensive Aircraft Encounter Model of the National Airspace System," *Lincoln Laboratory Journal*, vol. 17, no. 2, pp. 41–53, 2008, [Online]. Available: https://pdfs.semanticscholar.org/4086/9e6358bded8c07a7e5480facee4223fa0a29.pdf

[37] "Airplane Flying Handbook," Federal Aviation Adminstration, FAA-H-8083-3B, 2016. [Online]. Available: https://www.faa.gov/regulations_policies/handbooks_manuals/aviation/airplane_handbook/

[38] C. Serres *et al.*, *mit-ll/degas-core: Initial Release*. Zenodo, 2020. doi: 10.5281/zenodo.4323620.

[39] M. G. Wu *et al.*, "Detect-and-Avoid Closed-Loop Evaluation of Noncooperative Well Clear Definitions," *Journal of Air Transportation*, vol. 28, no. 4, pp. 195–206, 2020, doi: 10.2514/1.D0199.

[40] C. Chen *et al.*, "Defining Well Clear Separation for Unmanned Aircraft Systems Operating with Noncooperative Aircraft," in *AIAA Aviation 2019 Forum*, Dallas, Texas, Jun. 2019, pp. 1–14. doi: 10.2514/6.2019-3512.

[41] M. G. Wu, A. C. Cone, S. Lee, C. Chen, M. W. Edwards, and D. P. Jack, "Well Clear Trade Study for Unmanned Aircraft System Detect And Avoid with Non-Cooperative Aircraft," in *2018 Aviation Technology, Integration, and Operations Conference*, American Institute of Aeronautics and Astronautics, 2018. doi: 10.2514/6.2018-2876.

[42] A. Weinert, S. Campbell, A. Vela, D. Schuldt, and J. Kurucar, "Well-Clear Recommendation for Small Unmanned Aircraft Systems Based on Unmitigated Collision Risk," *Journal of Air Transportation*, vol. 26, no. 3, pp. 113–122, 2018, doi: 10.2514/1.D0091.

[43] A. J. Weinert, "An information theoretic approach for generating an aircraft avoidance Markov decision process," Boston University, Boston, MA, 2015. Accessed: Sep. 11, 2019. [Online]. Available: https://open.bu.edu/handle/2144/15208

[44] L. E. Alvarez, J. C. Jones, A. Bryan, and A. J. Weinert, "Demand and Capacity Modeling for Advanced Air Mobility," in *AIAA AVIATION 2021 FORUM*, American Institute of Aeronautics and Astronautics. doi: 10.2514/6.2021-2381.

[45] L. Wang, P. Lucic, K. Campbell, and C. Wanke, "Helicopter Track Identification with Autoencoder," in *2021 Integrated Communications Navigation and Surveillance Conference (ICNS)*, Apr. 2021, pp. 1–8. doi: 10.1109/ICNS52807.2021.9441606.

[46] H. Huang *et al.*, "Aircraft Type Recognition Based on Target Track," *J. Phys.: Conf. Ser.*, vol. 1061, p. 012015, Jul. 2018, doi: 10.1088/1742-6596/1061/1/012015.

[47] D. Bertsimas and S. S. Patterson, "The air traffic flow management problem with enroute capacities," *Operations research*, vol. 46, no. 3, pp. 406–422, 1998, doi: 10.1287/opre.46.3.406.